Faculdade de Engenharia da Universidade do Porto

Instituto de Ciências Biomédicas Abel Salazar da Universidade do Porto

Hydroxyapatite based antibacterial biocomposite for bone regeneration

by

Laura José Costa Henriques

Dissertation for the Master Degree in Bioengineering – Molecular Biotechnology

Supervisor: Prof. Susana R. Sousa (ISEP)

Co-supervisor: Prof. Valentina F. Domingues (ISEP)

Porto, June 2019

© Laura Costa, 2019

"There will be obstacles. There will be doubters.
There will be mistakes. But with hard work…
There are no limits."

(Michael Phelps)

Abstract

Bone regenerative therapies expansion reflects the significant increase in bone diseases, such as bone infections, bone tumors, and bone loss. In addition, the lack of antibacterial materials for bone regeneration represents a significant clinical demand, since microorganisms are prone to attach to surfaces, leading to the development of implant-related infections, that can result in implant failure.

Bacterial adhesion to an implant surface is a dynamic and complex process that strongly depends on the physicochemical properties of medical devices. Once a microorganism attaches to a biomaterial surface, starts division and colonizes the surface, producing a polysaccharide layer that will lead to biofilm formation. Device-associated infections are very difficult to treat due to the microenvironment that protects the bacteria against the host immune system and antibiotics, representing the need for new therapeutic agents to control bacterial infections.

Hydroxyapatite (HAp) ceramics have been widely used in clinical applications due to chemical similarity to bone as well as to their exceptional biocompatibility, bioactivity, osteoconductivity, and osteoinductive properties. Therefore, there is an interest in the use of ceramic-based composites that possess antimicrobial activity. The integration of magnesium oxide (MgO) with medical devices can provide biomaterials with sustainable antibacterial properties while mitigating the toxicity concern regarding burst of high concentrations of this metal oxide. MgO is biodegradable in the body and dissociate into magnesium (Mg^{2+}) ions that are beneficial for tissue healing.

In the present work, a granular composite that brings together the favorable biological characteristics of nanostructured hydroxyapatite with the antimicrobial activity of MgO was evaluated.

Surface characterization of the materials was performed by scanning electron microscopy, showing that higher sintering temperatures resulted in densification and loss of nanostructure. Degradation tests were assessed using the ISO 10993-14 standard and in a simulated body fluid (SBF) solution. The antibacterial activity of the spherical granules was investigated against *Staphylococcus aureus*, a Gram-positive bacteria known to cause various infections in humans. It was observed that lower sintering temperatures enhances the degradation loss releasing more MgO. Results also suggested the high efficacy of MgO as a potential antibacterial agent against the bacteria tested and that materials sintered at lower temperatures shown superior bactericidal efficiencies. The mechanism of antibacterial action of MgO was investigated through reactive oxygen species quantification using dichlorofluorescein assay, showing that the materials containing MgO (3% weight) were able to produce those reactive species. The material cytotoxicity was evaluated through the resazurin metabolic assay and showed that the granules allowed MC3T3-E1 cell proliferation over time.

These results suggested that the inclusion of antimicrobial agents, such as MgO, into spherical granules of HAp provides the possibility to promote bone tissue regeneration while inhibiting bacterial adhesion and consequently bacterial infection.

Key-words: Bone regeneration, biomaterial, hydroxyapatite, implant-related infections, magnesium oxide, antibacterial composite

Resumo

A expansão das terapias de regeneração ósseas reflete o aumento significativo de doenças ósseas, como infeções, tumores e perda óssea. Além disso, a falta de materiais antibacterianos para regeneração óssea representa uma necessidade clínica significativa, uma vez que os microrganismos tendem a ligar-se a vários tipos de superfícies, incluindo as de dispositivos médicos, levando assim, ao desenvolvimento de infeções que podem resultar na falha do implante. A adesão bacteriana na superfície de um implante é um processo dinâmico e complexo que depende fortemente das propriedades físico-químicas dos dispositivos médicos. Depois do micro-organismo aderir à superfície do biomaterial, este divide-se e coloniza a superfície, produzindo uma camada de polissacarídeos que leva à formação de biofilmes. Infeções associadas a dispositivos são muito difíceis de tratar devido ao microambiente que protege as bactérias contra o sistema imune do hospedeiro e antibióticos, representando a necessidade de novos agentes terapêuticos para o controlo de infeções bacterianas.

Materiais cerâmicos de hidroxiapatita (HAp) têm sido amplamente utilizados em aplicações clínicas, devido à similaridade química com o osso, e também pela biocompatibilidade, bioatividade, osteocondutividade e propriedades osteoindutivas. Deste modo, há um grande interesse na utilização de materiais compósitos à base de cerâmicos que possuam atividade antimicrobiana. A integração de óxido de magnésio (MgO) com dispositivos médicos pode fornecer aos mesmos, propriedades antibacterianas sustentáveis e ao mesmo tempo, diminuir a preocupação com a toxicidade, relacionada à exposição de altas concentrações do MgO, pois é biodegradável no corpo, dissociando-se em iões de magnésio (Mg^{2+}) que são benéficos para a cicatrização de tecidos.

No presente trabalho, avaliou-se um compósito granular que reúne as características biológicas favoráveis da hidroxiapatita nano-estruturada, com a atividade antimicrobiana do óxido de magnésio. A caracterização da superfície dos materiais foi realizada por microscopia eletrónica de varrimento, demostrando que temperaturas de sinterização maiores resultaram numa densificação e perda de nano-estrutura por parte do material. Os testes de degradação foram avaliados sob a orientação ISO 10993-14 e também realizados numa solução de fluido corporal simulado (SBF). A atividade antibacteriana dos grânulos esféricos foi investigada contra *Staphylococcus aureus*, uma bactéria Gram-positiva conhecida por causar várias infeções ósseas em humanos. Foi observado que temperaturas de sinterização menores aumentam a perda de massa e levam à libertação de maiores quantidades de MgO. Os resultados também sugeriram a alta eficácia do MgO como agente antibacteriano contra a bactéria testada, sendo que os materiais sinterizados a temperaturas mais baixas mostraram ser mais bactericidas. O mecanismo de ação antibacteriana do MgO foi investigado através da quantificação de espécies reativas de oxigênio (ROS) utilizando um ensaio de diclorofluoresceína. Este mostrou que os materiais que continham óxido de magnésio na sua composição (3% peso) foram capazes de produzir essas espécies reativas. A citotoxicidade do material foi avaliada através de um ensaio metabólico com resazurina e demonstrou que os grânulos permitiram a proliferação de células MC3T3-E1 ao longo do tempo. Estes resultados sugerem que a inclusão de agentes antimicrobianos, como o MgO, em grânulos esféricos de hidroxiapatita possibilitam a regeneração do tecido ósseo, ao mesmo tempo que inibe a adesão bacteriana e, consequentemente, a infeção bacteriana.

Palavras-chave: regeneração óssea, biomaterial, hidroxiapatita, infeções associadas a implantes médicos, óxido de magnésio, compósito antibacteriano

Acknowledgments

First of all, I would like to thank my supervisor, Professor Susana Sousa, and my co-supervisor, Professor Valentina Domingues, for having accepted me as a master student, for all the support and patience throughout this process. I am thankful for all the valuable suggestions they gave me, and for sharing their knowledge and experience.

I also want to specially thanks Catarina Coelho, for all the great advice, accompaniment and kindness support during all this journey. I appreciate all the help provided and for always saying the right words at the right time, either for encouragement or stimulus.

To all my team colleagues and friends, in the *Biocomposites* group and in MIB, thank you for your incredible help, company and friendship.

My sincere acknowledgements to i3S for having accepted me in its laboratories and for all the facilities I used in my dissertation. My acknowledgments also to FEUP and ICBAS for receiving me and for all the learning and skills provided.

Finally, to my family, in special my parents and sisters, thank you for all the unconditional love, support and guidance during these five years, for always believing in me and pushing me to my best. A special thanks to my sister Alice for the companionship, encouragement and tireless support through the whole process. And thanks, to my love and best friend, for the affection, comprehension, and for always putting a smile on my face, even from a distance, no matter how difficult the week had been. To all of them my sincere thanks! Without you, this would never be possible!

Table of Contents

Abstract v

Resumo vi

Acknowledgments vii

Table of Contents ix

List of figures xi

List of tables xiii

List of abbreviations xv

1. Literature review 1

1.1. Bone tissue and regeneration 1

1.1.1. Bone structure and composition 1

1.1.2. Bone regeneration 3

1.2. Biomaterials for bone regeneration 4

1.2.1. Hydroxyapatite 6

1.2.2. Biocomposites 7

1.3. Orhopedic implant-related infections 8

1.3.1. Bacterial adhesion and biofilm formation 9

1.3.2. Infections-related bacteria 11

1.4. Antibacterial agents 13

1.4.1. Metal oxides 14

1.4.1.1. Magnesium oxide 15

1.5. Objective and context of the work 18

1.6. Structure of the dissertation 19

2. Materials and Methods 20

2.1. Test materials 20

2.2. Surface morphology characterization 20
2.3. Degradation tests and magnesium release from the biocomposite 20
2.4. *In vitro* microbiological assays 21
2.4.1. Bacteria and culture conditions 21
2.4.2. Antibacterial activity of the biocomposite granules 21
2.4.3. Initial bacterial cell adhesion tests 22
2.4.4. ROS detection and quantification 22
2.5. *In vitro* cytocompatibility assay 24
2.5.1. Cell culture and sample preparation 24
2.5.2. Resazurin assay 24
2.6. Statistical analysis 25

3. Results and Discussion 26

3.1. Surface morphology characterization 26
3.2. Degradation tests and magnesium release from the biocomposite 29
3.3. *In vitro* microbiological assays 38
3.4. *In* vitro cytocompatability test 44

4. Conclusions and future perspectives 47

References 51

Annexes 61

Annex A: Magnesium calculations from the degradation tests 61

List of figures

Figure 1 - Schematic representation of bone structure at different hierarchical levels (Dumont, Kaysser-Pyzalla, Kostka, Sander, & Borbely, 2009). 1

Figure 2 – Bone remodeling process, involving the cooperation of osteoblast and osteoclasts (Fuchs et al., 2019). 3

Figure 3 – Hydroxyapatite main properties. 6

Figure 4 – Interaction between the microorganism, the biomaterial and the host in the pathogenesis of implant-associated infections (Adapted from Trampuz and Widmer (2006)) 9

Figure 5 – Representation of microbial adhesion to a biomaterial substrate. In phase I, adhesion of planktonic bacteria involves reversible cellular association with the surface. During Phase II, bacteria undergo irreversible molecular bridging with the substrate through cell surface adhesin compounds. After approximately 1 day, certain bacterial species are capable of secreting a protective exopolysaccharide matrix (biofilm) that protects the sessile from host defenses and systemically-administered antibiotics (Hetrick & Schoenfisch, 2006). 10

Figure 6 – Deaths attributable to antimicrobial resistance (AMR) every year by 2050 compared to other major causes of death (*Antimicrobial Resistance: Tackling a crisis for the health and wealth of nations*, 2014). 14

Figure 7 – Schematic illustration of the Gram-positive and Gram-negative cell membrane. 16

Figure 8 – Schematic illustration of the procedure performed in the degradation tests. 21

Figure 9 – Schematic representation of the initial bacteria adhesion protocol. 22

Figure 10 – Detection of ROS with the $DCFH_2$-DA probe. 23

Figure 11 – Schematic illustration of the main steps implemented in the resazurin assay. 24

Figure 12 - SEM images of the HAp/MgO granules at low magnifications, representative for all the materials used in this dissertation a) 250x magnification allows the visualization of the spherical shape and size, and b) 2000x magnification evidences the spherical microaggregates of HAp in the surface of each granule. The sample used was the 3 wt% MgO 1100 °C. 26

Figure 13 - EDS analysis. a) SEM image of a detailed zone in the 3 wt% MgO 1100 °C sample at 10000x magnification with two distinct zones highlighted in red, one corresponding to HAp (Z1) and other to magnesium oxide (Z2) as proved by b) the EDS spectrum. 27

Figure 14 - Weight loss % results of the HAp/MgO samples in a) Tris-HCl solution and b) SBF solution during three time-points (day 1, 14 and 28). Results are expressed as the mean ± SD and the experiment was performed in triplicate. 30

Figure 15 - ICP-MS analysis of the HAp/MgO granules in a) Tris-HCl solution and b) SBF solution during all time-points of the experience. For the values presented in b) the concentration of magnesium derived from the magnesium chloride hexahydrate ($MgCl_2 \cdot 6H_2O$) in the SBF solution was taking in consideration (Demonstration in Annex A.1). Each data point represents the mean ± SD and the experiment was performed in triplicate. 31

Figure 16 - Weight percentage equivalent to the magnesium oxide content released from the 3 wt% MgO granules during the degradation tests in a) Tris-HCl solution and b) SBF solution. The values are expressed as the mean percentage ± SD. An example of the calculations performed, and the values obtained are presented in the Annex A.2. 32

Figure 17 – EDS analysis of the 3 wt% MgO 1100 °C samples after 1-day immersion in SBF. a) SEM image of a HAp nanoparticle at 40000x magnification where it visible the magnesium oxide particles reaching the surface and the depressions left by them. b) EDS spectrum of the two highlighted zones in the SEM image indicates the existence of oxygen and magnesium, confirming the presence of MgO at the surface of the nanoparticle (Z1).....34

Figure 18 - Antibacterial effect of granules after 24 h incubated with *S. aureus*. Population of planktonic bacteria results are expressed in CFU/mL and * represents a significant reduction between the pure HAp granules (0 wt% MgO) and the 3 wt% MgO granules ($p < 0.05$). Each data point represents the mean ± SD of 3 independent experiments performed in triplicate (n = 3). 39

Figure 19 - Initial bacterial adhesion studies. Number of adherent bacteria cells in the materials after 1 h incubation is represented in CFU/mL. Results are expressed as mean ± SD (n=5) 40

Figure 20 – ROS production by *S. aureus* bacterial cells upon 24 h incubation with the granules (G1) during 1, 2, 3 and 4 h incubation either with a) $DCFH_2$-DA or b) $DCFH_2$ (20 μM final concentration). TSB medium was used as negative control and TBHP as positive control. Results are expressed in terms of relative fluorescence units (RFU) and background fluorescence was taking into consideration. The experiment was done in triplicate. * represents a significant difference when compared with negative control, and # symbolizes a statistical difference when compared with the positive control ($p < 0.05$).....42

Figure 21 – $DCFH_2$ assay for the detection of ROS produced by the materials alone (bacterial-free system) or by *S. aureus* incubated with the materials for 24 h, upon 1 h incubation with 20 μM of $DCFH_2$. Both material sizes were tested (G1 and G2) and the study was performed in triplicate. Results are expressed in terms of relative fluorescence units (RFU) and corrected for background fluorescence. * represents a significant difference when compared with negative control (TSB), and # symbolizes a statistical difference when compared with the positive control (TBHP) ($p < 0.05$).....43

Figure 22 – Metabolic activity of the MC3T3-E1 osteoblasts seeded with the test materials at a) day 3, b) day 7 and c) day 14. Resazurin fluorescence was measured 3-4 h post-incubation. * represents significant differences compared to the negative control (TCPS).....45

List of tables

Table 1 – Etiology of orthopedic infections (strains sampled in the period 2007-2011) (Montanaro et al., 2011). 12

Table 2 - SEM images of the HAp/MgO materials used in the study at high magnifications (10000x and 40000x). Surface morphology changes with the incorporation of MgO and also with the sintering temperature applied in the fabrication process. It is possible to observe MgO aggregates in the middle of HAp particles and also MgO nanoparticles on the surface of the HAp (black arrows). 28

Table 3 – SEM images of the 3 wt% MgO 1100 °C samples immersed in Tris-HCl at three different time-points (day 1, 14 and 28). The MgO particles are represented with black arrows and the cavities presumed to be left by these particles highlighted by red arrows. 33

Table 4 - SEM images of the 3 wt% MgO 1100 °C samples after 1, 14 and 28 of immersion in SBF solution. As before, the black arrows indicate the particles of MgO and the red arrows the cavities after their release. 35

Table 5 – SEM images at high magnification (40000x) of the HAp/MgO spherical granules sintered at 1100 °C at the end of the immersion tests in Tris-HCl and SBF. The black arrows pointed out the magnesium oxide and the red arrows the depressions left by those. 37

Table 6 – Weight percentage equivalent to the magnesium oxide content released from the 3 wt% MgO granules during the degradation tests in both solutions. The values are expressed as the mean percentage ± SD. 62

List of abbreviations

α-MEM	Alpha minimum essential medium
AFM	Atomic force microscopy
ATCC	American Type Culture Collection
ALP	Alkaline phosphatase
AMR	Antimicrobial resistance
ANOVA	One-Way analysis of variance
CFU	Colony-forming units
DCF	2',7'-dichlorohydrofluorescein
$DCFH_2$	2',7'-dichlorodihydrofluorescein
$DCFH_2$-DA	2',7'-dichlorodihydrofluorescein diacetate
DMF	Dimethylformamide
DMSO	Dimethyl sulfoxide
E. coli	*Escherichia coli*
ECM	Extracellular matrix
EDS	Energy dispersive X-ray spectroscopy
FBS	Fetal bovine serum
G1	Small granular samples (0.5-1 mm)
G2	Larger granular samples (1-2 mm)
HAp	Hydroxyapatite
ICP-MS	Inductively coupled plasma-mass spectrometry
ISO	International organization for standardization
m	Weight
M	Molar mass

MC3T3	Osteoblastic cell line derived from mouse calvaria
MRSA	Methicillin-resistant *Staphylococcus aureus*
n	Number of moles
nHAp	Nanostructured hydroxyapatite
nMgO	Magnesium oxide nanoparticles
OD	Optical density
PBS	Phosphate buffered saline
PIA	Polysaccharide intercellular adhesin
PJI	Prosthetic joint infections
RFU	Relative fluorescence units
ROS	Reactive oxygen species
RPM	Rotations per minute
S. aureus	*Staphylococcus aureus*
SBF	Simulated body fluid
SD	Standard deviation
SEM	Scanning electron microscopy
SOD	Superoxide dismutase
TBHP	*tert*-Butyl hydroperoxide
TCPS	Tissue culture polystyrene
Tris-HCl	Tris hydrochloride
TSA	Tryptic soy agar
TSB	Tryptic soy broth
wt%	Weight percentage

1. Literature review

1.1. Bone tissue and regeneration

1.1.1. Bone structure and composition

Bone is a specialized connective tissue with distinguished elasticity and flexibility, that is mainly responsible for mechanical support, protection, and motion of our body. It also plays an important role in maintaining homeostasis, since it is the main calcium (Ca^{2+}) reservoir in the organism. At a macroscopically level, the bone tissue can be divided into two main parts, an external layer of smooth, dense and continuous tissue called cortical or compact bone, and a highly porous core called trabecular or cancellous bone. Although with the same matrix composition, they differ in terms of structure, function, and distribution.

Cortical bone consists of closely packed osteons or Haversian systems, composed of collagen fibers, dominating at the nanometer level, and HAp crystals embed in the gaps (40 nm) present between collagen molecules. These crystals probably serve as nucleation sites for the biomineralization process and contribute to the stiffness of the bone that is essential for the mechanical roles of the tissue. Cancellous bone is softer and is composed of trabeculae interconnected with small, irregular cavities that home the bone marrow, committed with cell proliferation and differentiation, including the hematopoietic process (Fuchs, Thompson, & Warden, 2019; Gong et al., 2015; Porter, Ruckh, & Popat, 2009). The representation of the hierarchical structural organization of the bone is shown in Figure 1.

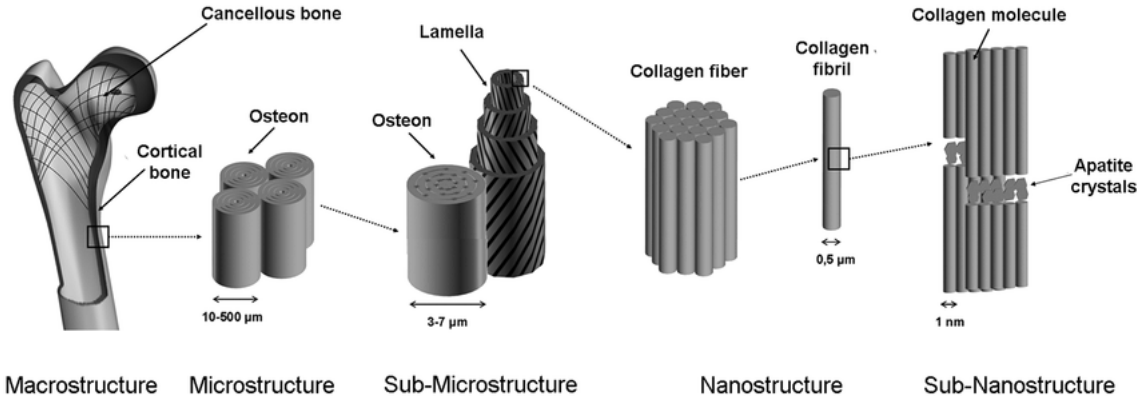


Figure 1 - Schematic representation of bone structure at different hierarchical levels (Dumont, Kaysser-Pyzalla, Kostka, Sander, & Borbely, 2009).

The extracellular structure of the bone comprises cells immersed in a highly complex matrix with an organic phase (25%), mainly collagen type I; an inorganic phase (65%), based on mineral hydroxyapatite (HAp) and water (10%). The organic component contains natural polymers such as collagen, glycoproteins, proteoglycans, and sialoproteins, which are important to control the growth and differentiation of cells involved in the bone remodeling process, whereas the inorganic component is responsible for providing appropriate structural support for loadings and also ion-storing (Bose & Tarafder, 2012; Fuchs et al., 2019).

At the cellular level, the skeletal tissue is a productive and metabolic active biological entity, mainly composed of four cellular elements: i) osteoblasts, ii) osteocytes, and iii) bone lining cells originated from mesenchymal stem cells (MSC); and iv) osteoclasts originated from hematopoietic progenitors (HSC). Osteoblasts are highly differentiated, non-migratory and the main cells responsible for bone formation since they synthesize and secrete organic matrix compounds. They also produce a fundamental enzyme, alkaline phosphatase (ALP), that play a determinant role in the induction of HAp deposition over extracellular matrix proteins, making ALP activity an excellent marker of osteodifferentiation and mineralization. Osteocytes are mature osteoblasts trapped in lacunae within the bone matrix and constitute the major cell type in the adult skeleton. Finally, osteoclasts are giant multinucleated cells derived from macrophages, highly migratory and responsible for the degradation of the bone, by the acidification of the microenvironment (they pump H^+ and Cl^-, originating HCl that dissolve the HAp) and secretion of collagenase and other proteases that degrade the demineralized extracellular matrix (Jayakumar & Di Silvio, 2010; Mackie, 2003).

Bone is one of the few tissues that has the ability to heal and regenerate itself, being highly vascularized and dynamic. The healing process involves three different phases: inflammation; repair; and remodeling (Ennis, Sui, & Bartholomew, 2013).

A complex network established by vascular canaliculi is responsible for the cell-mediated exchange of minerals and the detection of mechanical stresses that modulated bone formation or resorption. This remodeling process implies a cooperative action of osteoblasts and osteoclasts in response to physiological requirements. It consists of an organized sequence of events including osteoclast activation, resorption of the bone, reversal phase, osteoblasts activation and replacement of bone at the same anatomical site (Figure 2). The action of osteoblasts and osteoclasts are controlled by several enzymes and also paracrine signaling between cells, that can promote or inhibit the formation of new bone. The remodeling of the bone is responsible for bone growth during the development stages of the body, accommodation of changes in bone stress profiles and also, for maintaining skeletal integrity, healing and calcium regulation in the blood (Fuchs et al., 2019; Hadjidakis & Androulakis, 2006).

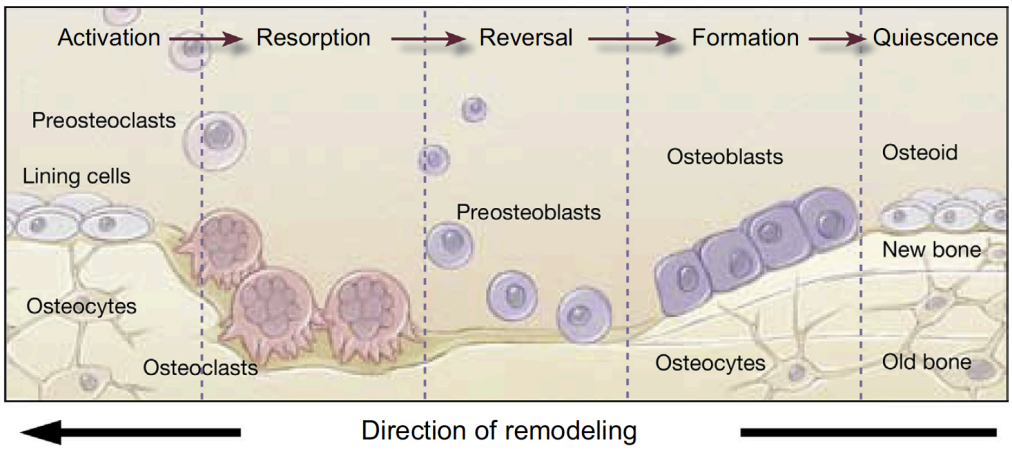


Figure 2 – Bone remodeling process, involving the cooperation of osteoblast and osteoclasts (Fuchs et al., 2019).

1.1.2. Bone regeneration

Bone regeneration is a complex, well-orchestrated physiological process of bone formation that involves a number of different cells and molecular signaling pathways in order to optimize skeletal repair and restore its function. Despite the superior healing and regenerative abilities of bone, for defects larger than a certain size ("critical size defect"), or in the occurrence of infections, the bone fails to heal and needs bone reconstruction with bone grafts. Such defects can occur in many musculoskeletal tissue diseases and injuries such as osteoarthritis, osteoporosis, fractures, tumors, trauma, congenital deformities, back pain and other spinal disorders, which are known to affect hundreds of millions of people across the world, especially the elderly population (Dimitriou, Jones, McGonagle, & Giannoudis, 2011; Giannoudis, Dinopoulos, & Tsiridis, 2005).

Nowadays, autologous bone grafts are considered the gold standard for the treatment of bone defects, due to their osteogenic, osteoinductive and osteoconductive potential, as well as their osteointegration and lack of disease transmission or immunogenicity. However, bone harvesting is associated with several clinical drawbacks, including risks of donor site morbidity, limited availability, chronic donor site pain, and secondary surgery cost. On the other side, allograft bone is more readily available but is limited by their potential infection and high nonunion rate with host tissues. Besides that, the use of bone grafts is also limited by the size of the defect and the viability of the host bed, since they are avascular and dependent on diffusion (Burg, Porter, & Kellam, 2000; Giannoudis et al., 2005; W. Wang & Yeung, 2017).

Therefore, to overcome these problems and promote a successful bone regeneration, suitable and biocompatible synthetic bone-graft substitutes have been designed and developed, in the last decades (Gong et al., 2015; Schieker, Seitz, Drosse, Seitz, & Mutschler, 2006; W. Wang & Yeung, 2017). However, the ideal material for optimal regeneration of damaged or lost tissues has not been identified yet.

1.2. Biomaterials for bone regeneration

According to Williams (1987), a biomaterial is defined as non-viable material used in a medical device, intended to interact with biological systems. As medical devices, it is meant, any product or equipment intended to be used for medical purposes, including biomaterials for bone regeneration.

An ideal biomaterial for bone regeneration should be highly biocompatible, bioactive, osteogenic, osteoinductive and osteoconductive, as well as, provide temporary mechanical support to the affected site, and enhance cellular activity towards scaffold-tissue integration (osteointegration). Besides that, they should be easily sterilizable (without losing their biochemical properties), degradable in a controlled and timely manner, with non-toxic products, and possess a highly interconnected porous network, to facilitate vascularization and bone tissue ingrowth (S. V. Dorozhkin, 2013; Matassi, Nistri, Chicon Paez, & Innocenti, 2011; Porter et al., 2009).

It is intended by biocompatibility the ability of a material to perform a specific application with an appropriate host response (Williams, 1987). As for the other properties, osteoconductive materials are those capable to support the growth of mature osteoblasts and direct apposition of bone, while an osteoinductive material has the ability to recruit undifferentiated, pluripotent cells and promote their osteogenic differentiation, which is crucial for the treatment of bone fractures and defects (Pietrzak, 2008). During the healing process, synthetic grafts need to be substituted by new bone and this process must occur without transient loss of mechanical support. For this reason, it is important to synchronize the biodegradation rate with the new bone formation rate (S. V. Dorozhkin, 2013).

Several engineering materials have been developed over the years, in order to meet the requirements mentioned before, including ceramics (aluminum oxide, carbon, calcium phosphates and glass-ceramics), natural and synthetic polymers (silicon, polymethyl methacrylate, polylactide, polyurethane, polyethylene), metals (titanium, titanium alloys, stainless steel, cobalt-chromium alloys) and composites (ceramic coatings on metal implants and ceramic-reinforced polymers). These graft substitutes are more than just fillers for bone defects, serving also as temporary matrices to provide chemical, mechanical and topographical cues to regulate cell behavior (Matassi et al., 2011; W. Wang & Yeung, 2017).

Depending on the application and biological requests, specific material may be more suitable than others, meaning that not all bone substitutes will act the same way and their performance in one clinical site may not necessarily be the same in another site. For example, metals seem to be the only group of materials appropriate for load-bearing applications, due to their mechanical properties. However, they present a limited ability to establish a direct bond with bone tissue compared to other materials such as calcium phosphates, that have a strong bonding capacity but lack of mechanical properties (Canillas, Pena, de Aza, & Rodríguez, 2017; Hannink & Arts, 2011).

Natural biodegradable polymers (collagen, gelatin, chitosan, and silk) and synthetic biodegradable polymers (polylactic acid, polyglycolic acid, polyurethane, and other copolymers) have shown to adequately support cell-driven growth and differentiation. They offer a great versatility, processability, and flexibility in property controls, although, these polymers use is

limited due to their insufficient mechanical strength, hydrophobic/bioinert surfaces and lowering of local pH, which is prejudicial to tissue formation (Oh, Oh, Appleford, & Ong, 2006; Raucci, Guarino, & Ambrosio, 2012).

Metallic biomaterials have been used for many years in a wide range of applications due to their tensile strength, toughness, and fracture and fatigue resistance. Porous titanium or tantalum are promising candidates to promote bone regeneration, due to their three-dimensional interconnected porosity, biocompatibility, durability and highly corrosion resistant (Matassi et al., 2011). However, metallic implants have issues related to metal-on-metal wear, metallic ion leaching, corrosion, and such other time-dependent degradation phenomena. Besides that, in general, they are considered bioinert and have poor osteoconductivity, not bonding adequately to the bone and presenting minimal interaction with the host mostly associated with protein adsorption and ultimately fibrous tissue encapsulation (Bose & Tarafder, 2012; Prasad et al., 2017).

In general, bioceramics are the most biocompatible among the hard tissue implant materials and have less effect on the immune system, being produced in a broader range of biochemical, mechanical and functional properties. For that reason, they have performed an important role in improving the quality and length of human life through their usage in biomaterials and medical devices. These ceramic materials can be classified as bioinert, when they have almost no influence in the surrounding living tissue, and/or bioactive, in the cases where they are capable of bonding with bone tissue.

Within the ceramics, calcium phosphate biomaterials are the most widely used bone substitutes mainly due to their bone-like structure and chemical composition, excellent biocompatibility, bioactivity, and tunable biodegradability. Other important advantages of CaP ceramics over autografts and allografts are their safety, predictability, easy processability, good cell attachment, non-immunogenic response, non-toxic degradation products, reduced local tissue morbidity, unlimited material availability and cost-effectiveness (Bose & Tarafder, 2012; Sergey V. Dorozhkin & Epple, 2002; Lobo & Arinzeh, 2010; Valletregi, 2004).

Besides that, another important property required for bone reconstruction, the interconnective porosity, can be introduced during the manufacturing process of CaP, which provide intimate and functional interfaces with neighboring bone, due to the increase of the surface area, allowing adhesion, proliferation, and differentiation of osteoprogenitor cells, as well as the revascularization, and subsequently ingrowth of new bone. However, these ceramics are known to have limited mechanical properties compared to bone, due to their brittleness and lower tensile strength, which makes them mostly unsuitable for application in load bearing areas (Hannink & Arts, 2011; Raucci et al., 2012).

CaP ceramics are widely used as bone substitutes in the form of: I) powders, II) granules, III) dense and porous blocks, IV) paste and V) composites. CaP synthesis involves the mixing of calcium and phosphate solution under acidic or alkaline solutions. However, not all CaP compounds produced are suitable for implantation in the body, the ones presenting a Ca/P ration less than 1 are not appropriate for biological implantation because of their high solubility. After conformation, they are usually processed by sintering at high temperatures with the exclusion of water vapor and subsequently molded by high-pressure compaction, with an increase of material densification for

higher temperatures. Thus, depending on temperature, impurities, and the presence of water, CaP can exist in different phases, and the most commonly used ones include hydroxyapatite (HAp), β-tricalcium phosphate (β-TCP) and combinations of HAp and β-TCP (Bose & Tarafder, 2012; S. V. Dorozhkin, 2013).

The biological response of implanted CaP follows a similar mechanism than fracture healing, involving a hematoma formation, inflammation, neovascularization, osteoclastic resorption, and a new bone formation. Just after implantation, proteins or bio-organic compounds start to be adsorbed onto the surface, affecting cells responses, like their proliferation and differentiation toward bone cells. Thus, the surface energy of the material might be important to attract particular proteins to the bioceramics surfaces, which will subsequently affect the affinity of the cell to the material. It is well known that the bioactivity and degradation behavior of these ceramics are directly dependent on the crystallinity, Ca/P ratio, and physical characteristics like porosity, pore size and distribution, and grain size, which also affect the cell behavior (Bose & Tarafder, 2012; S. V. Dorozhkin, 2013; Hench & Best, 2013; W. Wang & Yeung, 2017).

1.2.1. Hydroxyapatite

As mentioned before, HAp is the main inorganic component of natural bone (65 % of total bone mass), and for that reason it has been the synthetic calcium phosphate ceramic most extensively studied and used for bone replacement, mainly in the granular or pore structure form, with granules presenting the advantage of filling irregular and patient-specific bone defects (Bernhardt, Dittrich, Lode, Despang, & Gelinsky, 2013; Brydone, Meek, & Maclaine, 2010).

This phase is the most stable within a pH range of 4.2 - 8.0, and the least soluble one, presenting a Ca/P ratio of 1.67. It also presents excellent biocompatibility, osteoconductivity and osteoinductivity. When implanted *in vivo* it shows strong bonding with host bone, low resorption rates, and limited physical and mechanical properties **(Figure 3)**. Therefore, HAp alone is more often applied as a coating on implants or in sites with low mechanical stress (Denry & Kuhn, 2016; Samavedi, Whittington, & Goldstein, 2013).

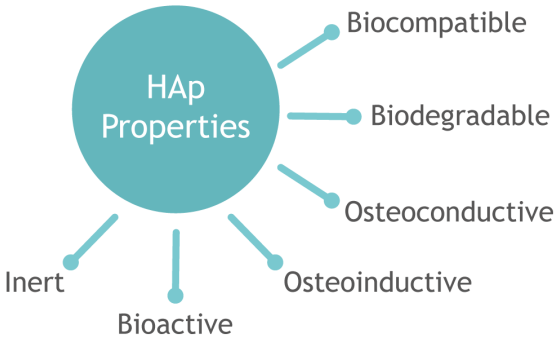


Figure 3 – Hydroxyapatite main properties.

Their physicochemical properties can be tailored via ionic substitutions, since the HAp crystalline structure includes several highly exchangeable sites. Many substitutions both cationic (substituting the calcium) and anionic (substituting the phosphate or hydroxyl groups) have been tried and tested, showing significant effects on thermal stability, solubility, osteoclastic and

osteoblastic response *in vitro*, and resorption rate and bone regeneration *in vivo*, even in very small amounts (Cacciotti, 2016; Campana et al., 2014).

The incorporation of a hierarchical architecture involving many length scales from the nano-level to generate strength, as well as micro-level structures to generate toughness, is essential in the design of stronger and resistance bone grafts substitutes. The ability to control topography and nanoscale chemistry offers interesting possibilities to stimulate the growth of new tissues through the development of new nanostructured scaffolds that mimic the nanostructure of body tissues. The term nanostructured refers to materials characterized by structural features of less than 100 nm in average size.

Nanostructured materials have been developed over the last years, inspired by the natural bone architecture, in order to better mimic the nanostructure organization of native extracellular matrix (ECM) and stimulating cell proliferation, differentiation, and migration, as well as guiding tissue regeneration. These nanoscale features include grooves, pits, wells, steps, pillars, pores, and ridges, and are an important determinant of stem cell lineage commitment. Nanostructured HAp relates to the natural bone HAp nanocrystals (osteo-mimetic architecture) and have been shown to improve bone regeneration due to high surface-to-volume ratios, bioresorbility, improved wettability and mechanical properties, and also increased protein adsorption, which can improve biomaterial osteoinduction and osteointegration, compared to microstructured HAp (S. V. Dorozhkin, 2013; Gong et al., 2015; P. Wang et al., 2014).

Several nanoHAp paste materials available on the market have shown to promote optimal tissue regeneration, being highly injectable which represents the possibility to use minimally invasive surgeries. Applications of HAp comprises bone substitutions, bone scaffolds, surface coatings, fillers in critical-sized defects, and controlled release systems (Bose & Tarafder, 2012; W. Wang & Yeung, 2017).

1.2.2. Biocomposites

Biocomposites are usually defined as engineered materials composed of two or more constituent materials, with significantly different physical or chemical properties. These materials contain at least one phase of a biological origin, that are combined to produce a new material with improved performance over individual constituent materials (Rudin & Choi, 2013). They are always heterogeneous, presenting two major categories of constituent materials: a matrix, or a continuous phase; and a dispersed phase that has the purpose to improve one or more properties of the matrix (Maiti, Jana, & Jana, 2017).

That is, composite approaches combine materials with different properties (e.g. osteoconductivity and osteoinductivity), using the advantages of the individual materials to achieve a better material class. The components used to produce a composite material must be biocompatible, non-immunogenic, non-toxic, and sterilizable. Since bone itself is a nanocomposite material of HA and collagen, considerable efforts have been made in order to design a polymer/ceramic composite material that mimics the microstructural features of bone (Matassi et al., 2011; Raucci et al., 2012).

Biodegradable polymers are frequently used in combination with CaP to diminish the brittleness and improve the mechanical properties of the scaffold. Polymer coatings on CaP scaffolds reduce their overall brittleness and increase their low strength, while CaP coatings on polymer scaffolds increase their bioactivity, promoting bone osteogenesis. Another composite approach is the coating of metallic materials with bioceramics and biocompatible polymers to improve the surface biocompatibility while maintaining their mechanical properties. For example, coatings of titanium surfaces with CaP have been assayed, in order to reduce the bioinert character of the metal and enhance bone osteointegration (Bose & Tarafder, 2012; Matassi et al., 2011; Yunus Basha, Sampath Kumar, & Doble, 2015).

As already mentioned, nanostructured materials exhibit enhanced mechanical, electrical, magnetic, and/or optical properties compared to their conventional micrometer-scale (or larger) counterparts, therefore a class of rapidly evolving nanostructured materials is that of nanocomposites in which nanometer-sized particles act as reinforcements in a matrix composed of conventional-size grains or amorphous material (De Santis, Guarino, & Ambrosio, 2019; Maiti et al., 2017) .

In general, the composite approach can produce new materials with better mechanical properties and bioactivity, promoting cell adhesion and improving the formation of new bone, and can exist in the form of powders, coatings, dispersions, or bulk materials. However, bone composite scaffolds developed so far have only been used in applications with non-load bearing and low load-bearing applications, including bone defect fillers, biomolecular delivery and maxillofacial treatments (De Santis et al., 2019; Yunus Basha et al., 2015).

1.3. Orhopedic implant-related infections

Applications of biomaterials in healthcare, such as in bone regeneration, have become widespread over the last three decades and these medical devices are increasingly being used in surgeries, with more than two million bone grafting procedures being performed annually worldwide (Campana et al., 2014; Marsh, Chamorro, & Chatzistavrou, 2019).

Infection is a major clinical complication in orthopedics since bone implantation of medical devices represents a specific opportunity for bacterial colonization, causing clinical complications for patients such as implant failure, several surgical procedures and, in severe cases, amputation and mortality. It also prolongs the hospital stay with antibiotic administration, and increases the healthcare costs (Ercan, Kummer, Tarquinio, & Webster, 2011; Katsikogianni & Missirlis, 2004; Perl et al., 2002).

These implant-associated infections result from the bacteria adhesion to biomaterials surfaces with subsequent biofilm formation at the implantation site, which is extremely resistant to host defense mechanisms and antibiotic treatment (Ribeiro, Monteiro, & Ferraz, 2012; von Eiff, Jansen, Kohnen, & Becker, 2005). The worst complications of orthopedic surgery and traumatology include osteomyelitis, septic arthritis and prosthetic joint infections (PJI), which are a tremendous burden for patients and global health care industry (Tande & Patel, 2014).

Depending on the sources of infectious bacteria, these bone tissue infections can be classified as hematogenous (bacteremia, bacteria already residing in the patient's body), or exogenous

(surgical equipment, resident bacteria on patient's skin, the operating room environment, clothing worn by health professionals) (von Eiff et al., 2005; Wright & Nair, 2010).

An infection can also be classified according to the time of manifestation after implantation. Early infection occurs within the first 3 weeks post-surgery and is mainly caused by highly virulent microorganisms like *Staphylococcus aureus* (*S. aureus*) or *Escherichia coli* (*E. coli*). Delayed infection takes place between 3 to 10 weeks post-operation and is typically caused by low virulence microorganisms such as coagulase-negative staphylococci (CoNS) or *Propionibacterium acnes*. These two stages are acquired through exogenously pathways. Finally, late infection manifests after more than 10 weeks post-implantation and its originated by hematogenous routes or recurrence of inadequately treated early infections (Zimmerli, 2014).

Implant-associated infections not only depends on the patient factors including obesity, rheumatoid arthritis, diabetes and immune-compromised status but also the infecting agents and the characteristics of the implanted medical device, such as size, shape, topography and material (Moriarty, Schlegel, Perren, & Richards, 2010; Rochford, Richards, & Moriarty, 2012; Trampuz & Widmer, 2006) **(Figure 4)**. As previously mentioned, the biomaterials must among other features, possess non-cytotoxic materials and mechanical stability. It is known for a long time that interactions of biomaterials with bacteria and tissue cells surface mostly depend on the surface and near-surface atomic structure and composition of implanted biomaterial, and it was suggested that these host cells and bacteria compete for positions on the implant's surface (Gristina, 1987).

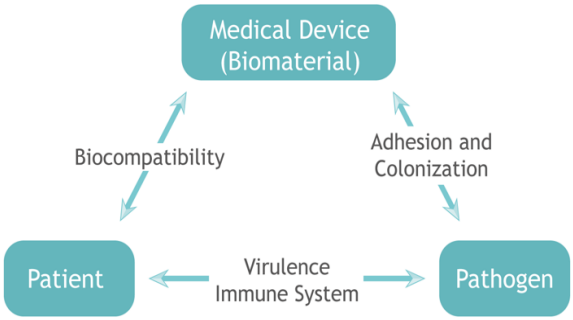


Figure 4 – Interaction between the microorganism, the biomaterial and the host in the pathogenesis of implant-associated infections (Adapted from Trampuz and Widmer (2006))

Concerning the mechanisms of infection, they are quite complex and vary with bacteria species. Generally, under favorable condition, it initiates with a reversible adhesion of the bacteria on the surface of the material, followed by a permanent attachment, involving protein-adhesin-receptors and forming a polysaccharide film where the bacteria multiplies and colonizes on the implant surfaces.

1.3.1. Bacterial adhesion and biofilm formation

Bacterial adhesion to an implant surface is the first and most important step in implant-associated infections. It is a dynamic and complex process, involving two different phases, an initial, instantaneous and reversible phase (phase I), followed by a time-dependent irreversible phase (phase II). This process is mediated by specific and non-specific interactions forces, with both

having an important role in the ability of the cell to attach to (or resist detachment from) the biomaterial surface (An & Friedman, 1998).

The reversible cellular association occurs within the first 1-2 hours post-implantation and it depends on the cell surface characteristics of the microorganism and on the nature of the biomaterial. These physical interactions are mediated through long (e.g. Brownian motions, van der Walls attraction forces, and electrostatic interactions) and short (e.g. chemical bonds, ionic and dipole interactions and hydrophobic interaction) range forces. Bacteria move to or are moved to a material surface by the so-called long-range interactions (non-specific, distances > 50 nm) and upon closer contact (< 5nm), short-range interactions become more important. The second and irreversible phase is characterized by molecular and cellular interaction between bacteria and substrate surfaces. It involves a stronger adhesion of bacteria to the biomaterial by the selective bridging function of bacterial surface polymeric structures (e.g. capsules fimbriae or pili, and slime). The functional part of these structures is called adhesins, which are responsible to mediate the adhesion of bacteria to various materials surfaces and protein tissues. Each bacteria presents multiple adhesins for different receptors on the surfaces of biomaterials or host tissue (An & Friedman, 1998; Hetrick & Schoenfisch, 2006; Katsikogianni & Missirlis, 2004).

Beyond phase II, certain bacterial strains are capable of forming a biofilm when provided an appropriate supply of nutrients (Figure 5). During this stage, bacteria secrete a layer of slime (exopolymers composed mainly of polysaccharides) that retains and protects them from the immune response, antibiotic therapy and physiologic shear (Francolini & Donelli, 2010; Hetrick & Schoenfisch, 2006).

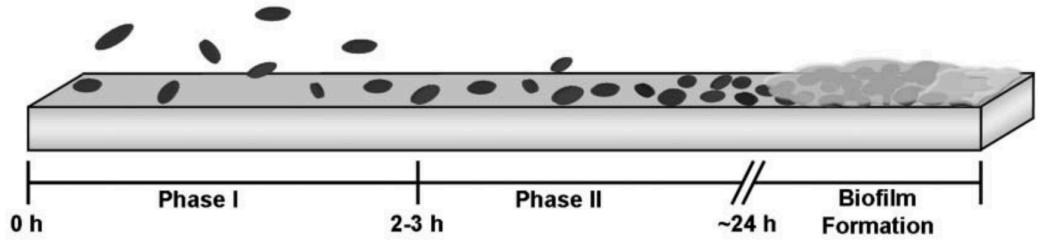


Figure 5 – Representation of microbial adhesion to a biomaterial substrate. In phase I, adhesion of planktonic bacteria involves reversible cellular association with the surface. During Phase II, bacteria undergo irreversible molecular bridging with the substrate through cell surface adhesin compounds. After approximately 1 day, certain bacterial species are capable of secreting a protective exopolysaccharide matrix (biofilm) that protects the sessile from host defenses and systemically-administered antibiotics (Hetrick & Schoenfisch, 2006).

Microbial adhesion process is affected by many factors including environmental factors, bacterial characteristics and material surface properties. Certain factors in the environment can influence bacterial adhesion, for example the temperature, exposure time length, bacterial density, chemical treatment, presence of serum or tissue proteins (e.g. fibronectin, albumin and fibrinogen) or/and antibiotics, and associated flow conditions (dominant factor), where higher shear rates decrease bacterial adhesion. As for the bacterial properties, since different bacterial species and strains present different physicochemical characteristics, they also adhere in a distinct manner. Bacteria with hydrophobic properties prefer hydrophobic material surfaces and the opposite likewise. The growth medium, pH and ionic strength of suspending buffer, bacterial age, and bacterial surface structure also influence the adhesion mechanism. Finally, for the

properties of the material, the chemical composition, surface charge, hydrophobicity, surface roughness and presence of specific proteins at the surface are important factors in the initial cell attachment process. Negatively charged surfaces, as well as hydrophilic ones, decrease bacterial adhesion. Increased surface area and depressions in roughened surfaces provide more sites for bacteria to adhere, whereas smooth surfaces do not favor bacterial colonization and subsequent biofilm formation (An & Friedman, 1998; Katsikogianni & Missirlis, 2004; Ribeiro et al., 2012).

Biofilm formation is a multistage process represented by the agglomeration, irreversibly adherence to a substrate and proliferation into colonies of the bacterial microorganisms. Bacteria growing in a biofilm enclose themselves within an extracellular polysaccharide matrix, and the cells in a biofilm (sessile cells) are phenotypically and physiologically different from non-adhered (planktonic) cells (Stewart & William Costerton, 2001).

Biofilm mode of growth includes a broad variety of bacterial defense strategies since bacteria act as a population instead of as individuals. Biofilm colonies are inherently resistant to both antimicrobial agents and host defenses and therefore, are the cause of many persistent bacterial infections. Major problems of biofilm formation include the possibility of chronic infection (reservoir of bacteria on the surface), the higher resistance to treatment with antibiotic, and the probability of chronic inflammatory response, since host responses and antimicrobial therapies are unable to eliminate bacteria growing in a biofilm (Francolini & Donelli, 2010; Suresh, Biswas, & Biswas, 2019; von Eiff et al., 2005).

Strategies to prevent biofilm formation and reduce the rate of implanted-related infections include systemic approaches controlling any bacterial invasion of sterile sites, inhibition of bacterial adhesion to the surface, interference with the signal molecules modulating biofilm development and lastly, disruption of the biofilm matrix.

1.3.2. Infections-related bacteria

The etiology of implant-associated infections is generally characterized by a broad variety of Gram-positive and Gram-negative bacteria as well as yeasts. Moreover, infection is typically related to *Staphylococcus* species, in particular, *S. aureus* and *Staphylococcus epidermidis* (*S. epidermidis*) **(Table 1)**. These species comprise two thirds of the implant-related infections reported and they represent the main causative agents of two major types of infection affecting bone, namely septic arthritis (Combs & Cox, 2018) and osteomyelitis (Hatzenbuehler & Pulling, 2011), and are also the most common pathogens in prosthetic joint infection (Yang et al., 2018).

Such infections cause serious morbidity and are often difficult to treat due to the ability of this microorganism to form small colonies and grow into biofilms that allow them to resist to traditional antibiotic therapies (Ribeiro et al., 2012; Yang et al., 2018).

Table 1 – Etiology of orthopedic infections (strains sampled in the period 2007-2011) (Montanaro et al., 2011).

Microorganism	All		MDs		No MDs	
	n	%	*n*	%	*n*	%
Staphylococcus aureus	95	35.1	52	31.7	43	40.2
Staphylococcus epidermidis	81	29.9	64	39.0	17	15.9
Pseudomonas aeruginosa	25	9.2	10	6.1	15	14.0
Enterococcus faecalis	11	4.1	4	2.4	7	6.5
Staphylococcus haemolyticus	9	3.3	3	1.8	6	5.6
Escherichia coli	8	3.0	4	2.4	4	3.7
Staphylococcus warneri	8	3.0	8	4.9	0	0.0
Staphylococcus hominis	5	1.8	4	2.4	1	0.9
Streptococcus agalactiae	4	1.5	1	0.6	3	2.8
Proteus mirabilis	4	1.5	2	1.2	2	1.9
Staphylococcus lugdunensis	3	1.1	2	1.2	1	0.9
Acinetobacter baumannii	3	1.1	1	0.6	2	1.9
Enterobacter cloacae	3	1.1	2	1.2	1	0.9
Staphylococcus capitis	3	1.1	1	0.6	2	1.9
Enterococcus faecium	2	0.7	1	0.6	1	0.9
Morganella morganii	2	0.7	2	1.2	0	0.0
Staphylococcus cohnii	1	0.4	1	0.6	0	0.0
Corynebacterium striatum	1	0.4	0	0.0	1	0.9
Serratia spp.	3	1.1	2†	1.2	1‡	0.9
Total:	271		164		107	

†Serratia marcescens *and a still unresolved species of* Serratia.
‡Serratia liquefaciens.
MD: Medical devices.

Staphylococcus are Gram-positive, non-spore forming facultative anaerobes, with sizes in the range of 0.5-1.5 μm, represented by individual cocci that divide into planes to form grape-like clusters. They possess a family of adhesins (cell-surface adhesion molecules) that interact with ECM components to facilitate its binding to the bone matrix. These adhesins include fibronectin-binding proteins, fibrinogen-binding proteins, elastin-binding adhesin and collagen-binding adhesin that were already identified as critical virulence factors implicated in several stages of infection (early colonization, invasion, tissue localization, and cell internalization) (Chagnot, Listrat, Astruc, & Desvaux, 2012). The diversity of virulence factors provides nutrients required for survival in the host, along with microbial cell protection from the host immune system during injury formation.

S. aureus is the major opportunistic pathogen responsible for a number of community-acquired, nosocomial and biofilm-related infections worldwide (Tong, Davis, Eichenberger, Holland, & Fowler, 2015). Bacteremia due to *S. aureus* has been reported to be associated with mortality rates of 15%–60% (Ishikawa, Hoshino, & Furukawa, 2017).

Polysaccharide intercellular adhesin (PIA) was found in many *S. aureus* strains, which is required for biofilm formation (extracellular polysaccharide matrix) and bacterium-bacterium adhesion. This surface protein along with others and the teichoic acids play a vital role in the initial attachment of *S. aureus* to the host protein-coated surfaces. The main problem associated with staphylococcal biofilms is their resistance to host defense mechanisms and antibiotic therapy, due to the emergence of methicillin-resistant *S. aureus* (MRSA) strains and resistance to other classes of antibiotics (Francolini & Donelli, 2010; Montanaro et al., 2011; Stewart & William Costerton, 2001; Tong et al., 2015; Wright & Nair, 2010; Yang et al., 2018).

This acquired resistant is attributed to a variety of genetic mechanisms including the acquisition of extrachromosomal plasmids or additional genetic information in the chromosome via

transposons or other types of DNA insertion, and by mutations in chromosomal genes. For that reason, many efforts have been made for the prevention of *S. aureus* biofilms including antibiotics combinations, identification of new anti-biofilm agents (e.g. repurposed of existing drugs, metal chelators and sulfhydryl agents, nanoparticles, antimicrobial peptides (AMPS), enzymes as biofilm disrupting agents, phytochemicals), surface modifications of medical implants to hinder *S. aureus* adhesion and biofilm development, and lastly, laser shock waves, ultrasound and photodynamic therapy that act in synergism with antibiotics (Suresh et al., 2019).

Staphylococcus species are one of the leading causes of debilitating bone disease worldwide, a situation that shows no sign of abating. The increasing antibiotic resistance of staphylococci and other pathogenic bacteria combined with the increased opportunity for infection provided by escalating numbers of orthopedic surgical procedures will only serve to exacerbate the problem (Wright & Nair, 2010).

1.4. Antibacterial agents

Antibiotics are the current standard to kill bacteria-induced infections by affecting prokaryotic cell components, such as bacterial cell wall synthesis, translational machinery and DNA replication with an intention to prevent or eliminate biofilm production. Even though antibiotics and antifungals have been widely used in clinical practice, post-operative infections still occur, especially involving indwelling medical devices, and many of these infections and associated microbes are drug resistant (Gold, Slay, Knackstedt, & Gaharwar, 2018).

Current antimicrobial strategies have largely been developed in order to control acute infections caused by planktonic bacteria, however, they often fail to control bacteria in the biofilm mode of growth. Despite antimicrobial therapy, morbidity and mortality associated with bacterial infections previously mentioned, remain high, partially as a result of the ability of these organisms to develop resistance to virtually all antibiotics (Figure 6). Antibiotic resistance is attributed to the restricted penetration of antimicrobials and host defense cells into biofilms and the metabolic inactivity of starved bacteria in deep biofilm layers because of the limited diffusion of nutrients. This antibiotic resistance is acquired mainly due to the production of enzymes that can modify, degrade or even inactivate the antibiotic. Other mechanisms involve efflux pumps and target mutations (Combs & Cox, 2018; Stewart & William Costerton, 2001).

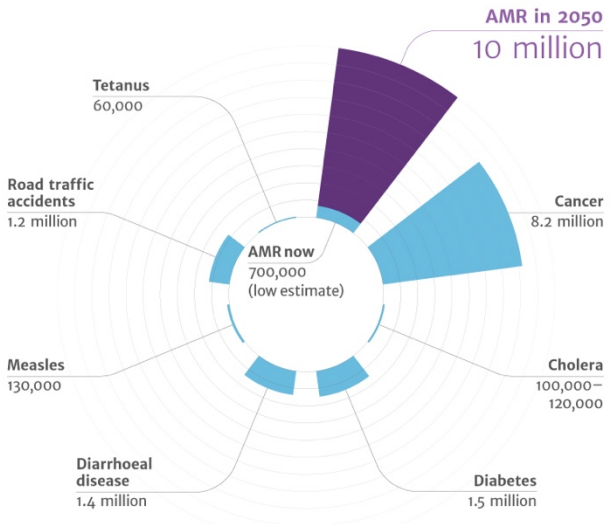


Figure 6 – Deaths attributable to antimicrobial resistance (AMR) every year by 2050 compared to other major causes of death (*Antimicrobial Resistance: Tackling a crisis for the health and wealth of nations*, 2014).

The resurgence of infectious diseases and the global rise of antibiotic resistance in pathogenic bacteria represents a serious threat to public health worldwide. Therefore research for novel therapeutic strategies is needed to identify and develop the next generation of drugs or agents to control bacterial infections (Gold et al., 2018; Ribeiro et al., 2012).

Antibacterial agents can be incorporated in the bulk or in the coating of a biomaterial, and they can be categorized as organic or inorganic, with the latter presenting the advantages of improved safety and stability (J. Sawai, 2003; Vidic et al., 2013).

Among inorganic antibacterial agents, silver has been extensively used because of its good antimicrobial action and low toxicity (Gosheger et al., 2004). Also, some metal oxides have been explored due to their intrinsic antimicrobial properties on a wide variety of Gram-positive and Gram-negative bacteria, with this effect being improved when these metal oxides are used as nanoparticles. Nanoparticles have small size and higher surface to mass ratio as already mentioned; therefore, it enhances the interaction and penetrative capabilities within the biofilm matrix (Gold et al., 2018; N. Jones, Ray, Ranjit, & Manna, 2008).

Metal nanoparticles like gold (Au), silver (Ag) and metal oxide nanoparticles, such as zinc oxide (ZnO), magnesium oxide (MgO), copper oxide (CuO), titanium dioxide (TiO_2) and calcium oxide (CaO) have been effectively recognized as antibacterial agents in the field of biomedical applications (Stoimenov, Klinger, Marchin, & Klabunde, 2002).

1.4.1. Metal oxides

Metal oxides such as TiO_2, ZnO, MgO, and CaO are of particular interest as they are stable under harsh process conditions and generally regarded as safe materials to human beings and animals (Stoimenov et al., 2002).

Metal and metal-oxide-based nanoparticles are able to provide long-term antibacterial and biofilm prevention. The antibacterial efficiency of nanomaterials is correlated with structural and physical properties like the size, shape and zeta potential (Gold et al., 2018). They have dimensions smaller than bacteria and higher surface area, leading to a strong, targeted and extended antimicrobial activity at small dosages (Das et al., 2018). The ability to prepare metal and metal oxide nanoparticles of specific size and shape allows the development of new antimicrobial agents.

Considerable antibacterial activity was observed for ZnO, MgO, CaO and TiO_2 nanoparticles and attributed to the ability of these nanoparticles to: (1) easily bind and damage the bacterial cell membrane, (2) penetrate the cell and bind to a specific target, and (3) formation of reactive oxygen species (ROS) on their surfaces that will lead to an enhancement of the intracellular oxidative stress (Gold et al., 2018).

Also, the antibacterial efficiency has been proven to be dependent upon the particle size (Yamamoto, 2001), the metal oxide concentration (J. Sawai, 2003), the microscopic arraignments of the nanoparticles (Ohira & Yamamoto, 2012), and also the bacteria species (Nguyen, Grelling, Wetteland, Rosario, & Liu, 2018; Jun Sawai, Igarashi, Hashimoto, Kokugan, & Shimizu, 1996). In general, smaller particle size and higher concentrations result in an increase in antibacterial activity (Yamamoto, 2001).

Some authors have reported zinc oxide as well as TiO_2 nanoparticles, as exhibiting greatest antibacterial activity among other metal oxides (Azam et al., 2012; N. Jones et al., 2008; Jun Sawai et al., 1996), however their use present some concerns regarding their toxicity due to the risks associated with heavy metals and their accumulation in the body. This being said, magnesium oxide represent an attractive alternative to heavy metals since it is an essential mineral for human health, being degraded and metabolized efficiently in the body, avoiding the excessive metal accumulation in the body (Aruoja et al., 2015; Nguyen et al., 2018).

1.4.1.1. Magnesium oxide

Magnesium oxide possesses excellent antibacterial activity towards different microorganisms, in addition to their high thermal stability, low cost and environmentally-friendly properties (Leung et al., 2014). Therefore, MgO nanoparticles (nMgO) alone or in combinations with other antimicrobials have been widely used and investigated in several fields and applications, including dentifrices (Yamamoto, Ohira, Alvarez, & Fukuda, 2010), food industry (Jin & He, 2011; Mirhosseini & Afzali, 2016), water purification (Bindhu, Umadevi, Kavin Micheal, Arasu, & Abdullah Al-Dhabi, 2016), nanoelectronics (Al-Hazmi et al., 2012), bone substitutes (Coelho, Araujo, Quadros, Sousa, & Monteiro, 2019) and other medical applications (Akram et al., 2018; Balraj, Senthilkumar, Vetha Potheher, & Arulmozhi, 2018; Wetteland, Nguyen, & Liu, 2016).

The antibacterial activity of the MgO nanoparticles was shown to be highly dependent on the particle size and concentration (Huang et al., 2005; Makhluf et al., 2005) and to act against both Gram-positive and Gram-negative bacteria (Krishnamoorthy, Manivannan, Kim, Jeyasubramanian, & Premanathan, 2012; Makhluf et al., 2005).

Jun Sawai et al. (2000) reported that the contact between MgO powders and bacterial cells are also an important factor for MgO-induced bacterial death. Besides that, the initial seeding densities of bacteria could be another factor affecting the antimicrobial efficiencies, since bacteria can behave differently at different seeding densities due to the quorum sensing (Nguyen et al., 2018).

The exact mechanism of nMgO action on bacteria is complex and not fully understood yet, however many theories have been purposed over the years, including elevated pH and Mg^{2+} ions, Ca^{2+} ion concentration, reactive oxygen species (ROS) production, membrane damage, quorum sensing and biofilm disruption (Nguyen et al., 2018).

The elevated pH and Mg^{2+} ions theory relates to the nMgO dissociation in bacterial culture which releases OH^- ions and Mg^{2+} ions, however some authors already reported that high pH treatment and Mg^{2+} ions did not affect the growth of the bacteria, meaning that this is not the main mechanism of killing for the antimicrobial activities of nMgO (Nguyen et al., 2018; Jun Sawai et al., 2000; Wetteland et al., 2016).

Moreover, Nguyen et al. (2018) suggested that the dissociation of nMgO to Mg^{2+} ions might have an implication on the Ca^{2+} ion concentrations in bacteria cultures. However, this correlation was not previously reported in literature and further research is needed to fully understand the specific roles of Ca^{2+} ions in the bacterial cultures with nMgO.

As for the membrane cell damage, it is believed that nMgO particles bind to the cell membrane to cause damage and kill the bacteria (Leung et al., 2014; Stoimenov et al., 2002). Nguyen et al. (2018) showed that the MgO nanoparticles affect the adhesion and morphology of the bacteria, with the disruption of the morphology of *E. coli* occurring more obviously than other bacteria. They observe membrane damage in the Gram-negative bacteria (e.g. *E. coli*) but not in the Gram-positive bacteria (e.g. *S. aureus*), which could be explained by the differences in their cell walls and membranes structures.

Gram-negative bacteria present a thinner layer of peptidoglycan with an outer membrane containing lipopolysaccharides (LPS), whereas Gram-positive bacteria have a thicker peptidoglycan cell wall without outer membrane and contain teichoic acids (Nguyen et al., 2018) **(Figure 7)**. For that reason, the nMgO could pass the thin defense layer of *E. coli* bacteria and bind to the cell membrane, causing shape distortion and cell death. The higher line of defense in Gram-positive bacteria might be due to the interaction of the positively charged nMgO particles with the negatively charged phosphate groups on the teichoic acid end. More nMgO may get trapped in the thick peptidoglycan layer and does not pass this thick defense layer to cause further damage (Huang et al., 2005).

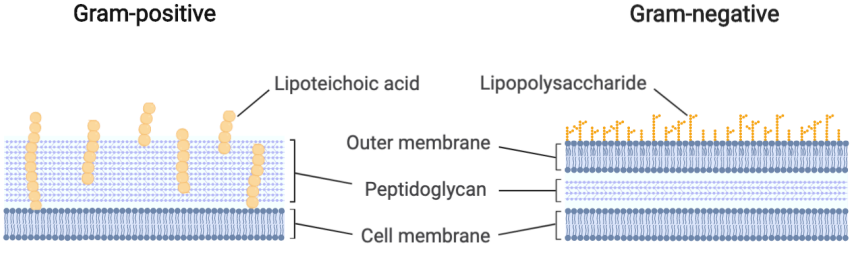


Figure 7 – Schematic illustration of the Gram-positive and Gram-negative cell membrane.

Regarding the ROS production, many reports stated this as the leading mechanism of antibacterial action of the nMgO (Das et al., 2018; Gold et al., 2018; Krishnamoorthy et al., 2012; Nguyen et al., 2018; Jun Sawai et al., 2000). It is possible that sequential oxidation/reduction reactions may occur at nMgO surface to produce reactive oxygen species such as superoxide radical (O_2^-), hydrogen peroxide (H_2O_2) and hydroxyl radical ($^{\bullet}OH$). The superoxide anion which is highly active can react with the carbon atom from carbonyl group in the peptide linkages in the cell wall of bacteria, eventually leading to the destruction of the bacteria (Krishnamoorthy et al., 2012).

Some bacteria can produce a cellular antioxidant defense enzyme, named superoxide dismutase (SOD) to neutralize the ROS. Besides that, *S.aureus* bacteria can produced another antioxidant enzyme, catalase, that neutralize the H_2O_2, hence the less susceptibility of this bacteria compared with *E. coli* (Karavolos, Horsburgh, Ingham, & Foster, 2003; Krishnamoorthy et al., 2012). Thus, ROS generated by nMgO could be neutralized by the SOD produced by bacteria. However, at higher concentrations of nMgO, more ROS might be produced, exceeding the capacity of the bacterial antioxidant defense system and the excess ROS could still cause damage to the bacteria (Nguyen et al., 2018). However, Leung et al. (2014) showed that nMgO inhibited the growth of *E. coli* without the presence of ROS, describing that the strong antibacterial activity of the MgO nanoparticles can be observed in the absence of any species of reactive oxygen species, and propose that the mechanism of action might be due to cell membrane damage.

Nguyen et al. (2018) suggested for the first time another mechanism for the antimicrobial action of nMgO, demonstrating their ability to target and disrupt biofilms of *S. epidermidis* bacteria. They proposed that these nanoparticles could chelate with proteins and enzymes, or act as a catalyst to degrade the extracellular matrix of the biofilm. In addition, they could also diffuse through the water channels in the biofilm matrix and disrupt the internal structure of biofilm.

In the literature, the concentration range of nMgO that has displayed antimicrobial effects is between 0.2-2.0 mg/mL nMgO (Nguyen et al., 2018). This range was also tested with bone marrow-derived mesenchymal stem cells (BMSCs) and it was showed that, at a lower concentration, the MgO nanoparticles increased BMSC adhesion density and proliferation, which is beneficial for bone healing and regeneration (Wetteland et al., 2016). This represents the possibility of incorporating nMgO into medical devices and implants, in order to reduce implant-associated infections. It can be used as an antimicrobial coating on indwelling medical devices or as an additive in polymer or ceramic-based composite materials for a medical device, where the nMgO could provide antimicrobial properties against infections without significant side effects.

1.5. Objective and context of the work

Bone is one of the few tissues that has the unique biological ability to self-regenerate its function upon injury. However, in cases of severe fractures or infections, a bone-graft substitute may be needed to restore their routine functions. Bone defects or diseases significantly affect patient's quality of life and regeneration of damaged bone is a major challenge in orthopedic surgery, requiring a 3D porous structure such as scaffolds or granules, where powders can be used as raw materials to obtain self-setting formulations. An ideal bone graft should be biocompatible, bioactive, osteoinductive, biodegradable, easy to fabricate, sterilizable and not cause any foreign body reactions upon implantation (Brydone et al., 2010; Dimitriou et al., 2011).

Natural bone is essentially a composite material, with cells embedded in a matrix composed of hydroxyapatite (HAp) mineral, and organic components, mainly collagen type I. It presents a hierarchical structure ranging from the microscale to the nanoscale, essential for its unique mechanical properties (Rho, Kuhn-Spearing, & Zioupos, 1998). Calcium phosphates (CaP) are the major constituent of bone mineral, and these ceramics present superior properties being bioinert, bioactive, and resorbable. They were proposed to treat various diseases, including bone fractures, and currently present the majority of commercial products directed to repair or regenerate damaged bone tissue (Canillas et al., 2017). Among the calcium phosphate ceramics, hydroxyapatite (HAp) has been widely used in medicine and dentistry for bone regeneration, non-loading sites and bone void fillers in the form of cement, granules or coatings, due to their chemical similarity to natural bone, biocompatibility, and osteoconductivity (Sergey V. Dorozhkin & Epple, 2002).

Microorganisms are known to attach to materials surfaces including those that are intended to be implanted for bone regeneration intentions, leading to implant-associated infections, that are most of the times difficult to treat due to biofilm formation and bacterial resistance to antibiotics. Moreover, these infections present several drawbacks including implant failure, high dose of antibiotic administration with prolonged hospitalization, many surgical procedures, loss of function, and more drastically, amputation. For that reason, alternative strategies to antibiotics have been developed to control these medical device-associated infections, including the use of metal oxides that had shown to possess strong antibacterial potential (Ercan et al., 2011; Nguyen et al., 2018).

HAp alone does not possess intrinsic antimicrobial properties, so combining this biocompatible material with a metal oxide that is capable to prevent bacterial infection would present a good strategy for successful bone reconstruction.

The aim of the present work was to evaluate the degradation and antibacterial activity of a composite that combines favorable biological characteristics of nanostructured hydroxyapatite (nHAp) and, simultaneously, possesses antibacterial activity as expressed by the magnesium oxide (MgO).

For the purpose of this work, the antibacterial potential of the composite granules composed by HAp and MgO nanostructured powders was evaluated using a Gram-positive bacteria *Staphylococcus aureus*, which is the most frequent etiologic agent of implant-related infections (Wright & Nair, 2010).

1.6. Structure of the dissertation

This dissertation is organized into four major chapters. In Chapter 1, the most relevant literature is revised, describing the state of the art of research involving hydroxyapatite and magnesium oxide for application as medical devices with antibacterial properties for bone reconstruction purposes. Also, it explores the rationale behind the present work and delineates its main objective. The next two chapters relate to the experimental work that was performed. Chapter 2 is dedicated to the description of materials, experiments and methodologies used, while Chapter 3 presents the results and their critical and concise analysis. Finally, the main findings of this work are summarized and recommendations for future studies are presented in the final chapter.

2. Materials and Methods

2.1. Test materials

The HAp/MgO composite granules used in this study were kindly provided by FLUIDINOVA, S.A. These materials are produced with HAp and MgO nanostructured powders and applying an ionotropic gelation method of sodium alginate in the presence of calcium ions. The granules were produced containing 3 wt% of MgO as previously optimized by Coelho et al. (2019). The final step of the production process involves a thermal cycle and different sintering temperatures were used, namely 900 °C, 1100 °C and 1300 °C. Granules with two different size ranges were also produced, namely 0.5-1 mm (G1) and 1-2 mm (G2). Prior to all tests, the granular samples were sterilized at 120 °C for 20 min through autoclave to avoid microorganism contamination.

2.2. Surface morphology characterization

The morphology of the samples was analyzed using a scanning electron microscope (SEM, FEI Quanta 400 FEG/ESEM) under several magnifications, with an accelerating voltage of 15 kV. The granules were fixed on aluminum sample holders using Carbon tape and then sputter coated (SPI Module) with a thin conductive film of Au/Pd alloy. Elemental composition of the granular samples was confirmed using energy dispersive x-ray spectroscopy (EDS, EDAX Genesis X4M detector attached to FEI Quanta 400 FEG/ESEM).

2.3. Degradation tests and magnesium release from the biocomposite

Degradation tests of the HAp/MgO spherical granules were conducted following the guidance "ISO 10993-14 – Biological evaluation of medical devices – Part 14: Identification and quantification of degradation products from ceramics", and also performed in a Simulated Body Fluid (SBF) solution, prepared as previously reported (Kokubo & Takadama, 2006). The granules were equally weighted in 15 mL Falcons and then Tris-HCl or SBF solution was added. They were incubated in an orbital shaker (Raypa) at 37 °C and 120 RPM, during 1, 3, 7, 14, 21 and 28 days. After completion of each incubation period, the solutions were filtered using a 0,22 µm filter and collected into Eppendorf tubes for further inductively coupled plasma-mass spectrometry (ICP-MS) analyses (performed by REQUIMTE, Nova University of Lisbon) to determine magnesium concentration. The remaining granules were dried in a vacuum oven for 24 h. After drying, Falcons were weighted with the respective lids. These steps are illustrated in Figure 8. The experiment was performed in triplicates. The weight loss rate was calculated as follows:

$$Weight\ loss\ (\%) = \frac{W_0 - W_t}{W_0} \times 100 \qquad (1)$$

where W_0 is the initial mass of the material before starting the incubation and W_t corresponds to the mass after a specific immersion time.

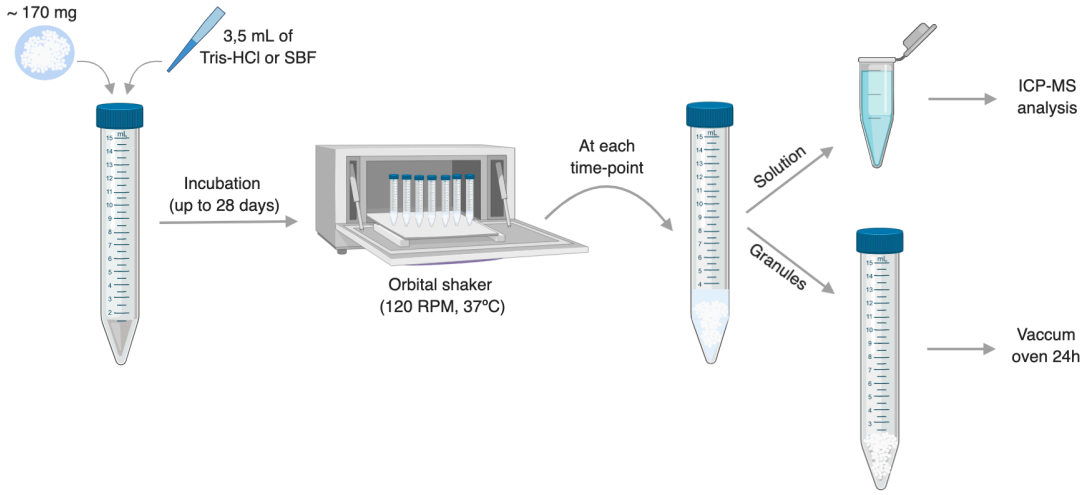


Figure 8 – Schematic illustration of the procedure performed in the degradation tests.

At the end of each experiment, samples of three different time points (day 1, 14 and 28) were also analyzed by SEM, to evaluate the surface degradation of the materials.

2.4. *In vitro* microbiological assays

2.4.1. Bacteria and culture conditions

S. aureus ATCC 33591 (American Type Culture Collection) was used to evaluate the antibacterial potential of the materials. The microorganisms were kept at -20 °C in a solution containing 70% tryptic soy broth (TSB) (Merck) and 30% diluted glycerol. Bacteria were inoculated from the frozen stock onto tryptic soy agar (TSA) (Liofilchem) plates for 18 h at 37 °C. Exponential phase cells were obtained by incubating one or two colonies, from the TSA plates, in 5-10 mL of TSB for approximately 3-4 h at 37 °C and 150 RPM.

2.4.2. Antibacterial activity of the biocomposite granules

The antibacterial activity of the HAp/MgO granules was evaluated as previously reported (Coelho et al., 2019). Briefly, bacterial isolates in exponential phase were used to prepare a suspension with an optical density at 600 nm (OD600) of 0.2, which corresponds to $1x10^8$ colony-forming units (CFU)/mL, and then diluted in TSB to obtain a cell density of $1x10^6$ CFU/mL. 200 µL of bacterial suspension was added to a 96-well plate containing 20 mg of granules per well and the plate was incubated for 24 h at 37 °C and 150 RPM. After incubation, new 96-well plates were prepared to perform a serial dilution step, adding 180 µL of 0.9 % sodium chloride (NaCl) (Sigma) into each well and 20 µL of the resulting suspensions into the first dilution wells. Then, the samples were serially diluted and aliquots of 10 µl of each sample were inoculated in TSA plates.

The number of colonies was counted after incubation at 37 °C overnight to determine the planktonic population of *S. aureus*. All experiments were performed in triplicate.

2.4.3. Initial bacterial cell adhesion tests

The influence of the morphology of the granules on bacterial adhesion was evaluated by initial (1 h) adhesion studies. To better evaluate the influence of the surface morphology, granules with 1-2 mm were used. As mentioned before, bacterial cells in exponential phase were diluted in TSB to obtain an initial suspension of $1x10^8$ CFU/ml and then 200 µL of this bacterial suspension was added to a 96-well plate containing 20 mg of the different granules per well. After 1 h incubation at 37 °C and 150 RPM, the bacterial suspension was removed, and the materials were washed 3 times with 0.9 % NaCl in order to remove any poorly adherent bacteria. Then, the granules were transferred to new wells, 200 µL of 0.9 % NaCl was added, and the 96-well-plate was sonicated for 15 min in an ultrasonic bath (Bandelin Sonorex Digitec), to release the adherent bacteria. Serial dilutions of the sonicated samples were prepared and inoculated in TSA plates at 37 °C overnight. The number of colonies was counted and bacterial adhesion on the surface of the granules was expressed in CFU/mL **(Figure 9)**. Three replicates per material were used in the experiments.

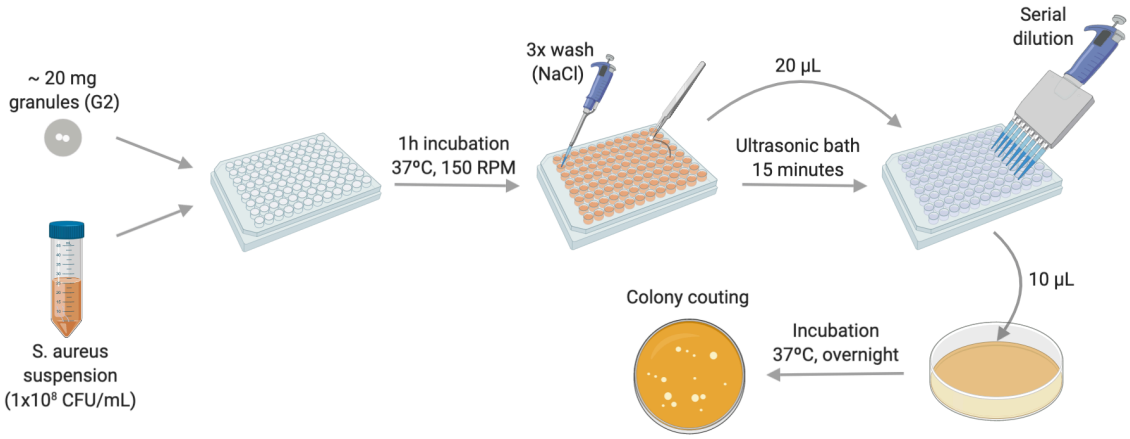


Figure 9 – Schematic representation of the initial bacteria adhesion protocol.

2.4.4. ROS detection and quantification

Reactive oxygen species (ROS) production in bacterial cells was evaluated using the chemical 2',7'-dichlorodihydrofluorescein diacetate ($DCFH_2$-DA) (Merck), which is a fluorescent probe widely used for more than 40 years (Chen, Zhong, Xu, Chen, and Wang (2010)). $DCFH_2$-DA itself is a non-fluorescent and cell-permeable molecule, unreactive toward oxidants. The dye diffuses into the cell membrane and is cleaved by intracellular esterases to form the hydrophilic 2',7'-dichlorodihydrofluorescein ($DCFH_2$) non-fluorescent product. Subsequent oxidation of the $DCFH_2$ generates the highly fluorescent 2',7'-dichlorohydrofluorescein (DCF), that is reactive toward oxidizing species, such as peroxide, hydroxide, and others reactive species within the cell, allowing the measurement of the ROS produced, through several fluorescence-based techniques (Chen et al., 2010; Eruslanov & Kusmartsev, 2010) **(Figure 10)**.

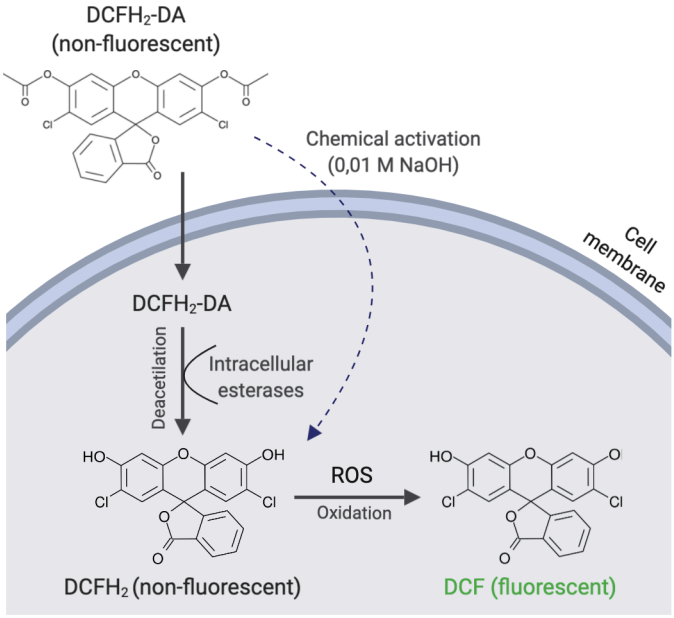


Figure 10 – Detection of ROS with the $DCFH_2$-DA probe.

To evaluate the ROS formation two different sizes of the materials were tested, the 0.5-1 mm (G1) and the 1-2 mm (G2). Two different methodologies were applied, one starting from the $DCFH_2$-DA itself, and other from the hydrophilic derivative ($DCFH_2$) which is normally used for cell-free studies. First, stock solutions of 1 mM $DCFH_2$-DA were prepared in 99 % ethanol and stored at -20 °C in the dark until use. Then, prior to each experiment, dichlorofluorescein ($DCFH_2$) was prepared from $DCFH_2$-DA by the method of Cathcart, Schwiers, and Ames (1983) by reacting 0.25 mL of 1.0 mM $DCFH_2$-DA in ethanol with 1 mL of 0.01 N NaOH, for 30 min. in the dark (chemical activation process). The mixture was then diluted with PBS to a working stock of 100 μM. When the study was conducted, the granules were washed once with TSB and bacterial suspensions with a cell density of $1x10^6$ CFU/mL were incubated with the materials for 24 h. After that, bacterial cell suspensions were collected to new wells in the 96-well-plate and 20 μM of $DCFH_2$-DA or $DCFH_2$ were added. This step was performed to avoid any possible effect of the materials in the fluorescence readings. *tert*-Butyl hydroperoxide (TBHP) was used as the positive control for ROS formation with a final concentration of 500 μM. Bacterial cells in TSB were also treated with the probe to serve as negative controls, as well as wells without bacterial cells (with and without the granular samples). Fluorescence was measured immediately after dye addition and every 1 h during 4 h with excitation and emission wavelengths of 485 and 528 nm respectively, using a microplate reader (SynergyMx, BioTek). Between measurements the micro-well plate was maintained in an incubator at 37 °C under dark conditions. Since baseline fluorescence varied from condition to condition and from experiment to experiment, the data presented represent the change from baseline (baseline fluorescence was subtracted from all values). Three samples per condition were used and the results are expressed in relative fluorescence units (RFU).

2.5. *In vitro* cytocompatibility assay

2.5.1. Cell culture and sample preparation

MC3T3-E1 osteoblasts were cultured in alpha minimum essential medium (α-MEM) (Sigma-Aldrich), supplemented with 10% fetal bovine serum (FBS) (Gibco) and 1% penicillin-streptomycin (Gibco), and incubated at 37 °C under a 5% CO_2 atmosphere.

For the *in vitro* cytotoxicity test four different samples were analyzed, corresponding to the 0 and 3 wt% MgO with sintering temperatures of 1100 °C and 1300 °C. Also, the two different sizes of the granules were used (G1 and G2). Before cell seeding, the granules were equilibrated in cell culture medium during 24 h at 37 °C.

2.5.2. Resazurin assay

Cell metabolic activity was quantified by the resazurin colorimetric assay. Resazurin (7-hydroxy-3H-phenoxazin-3-one 10-oxide) is a cell-permeable blue dye weakly fluorescent that is irreversibly reduced to resorufin, a pink and highly fluorescent compound, by viable cells with an active metabolism. This reduction is proportional to the number of living cells and can be quantified by spectrophotometers using appropriate filters (Riss et al., 2013 May 1 [Updated 2016 Jul 1]).

After equilibration in culture medium, the materials were placed in a 96-well-plate. Then a cell density of $1.3x10^5$ cells/mL was seeded on the different granules and incubated at 37 °C. Only cells with culture medium and cell-free systems (only materials in cell culture medium) were used as negative controls. After 3, 7 and 14 days of incubation, 10% resazurin was added to each well and the microplate was incubated for 3-4 h at 37 °C in dark conditions. Afterward, 100 μL of the solutions were transferred to a black 96-well-microplate and the fluorescence was measured at 530 nm excitation and 590 nm emission using a microplate reader (SynergyMx, BioTek). The remaining medium in the 96-well-plate was discarded, the materials were washed with phosphate buffered saline (PBS) twice and then 200 μL of new supplemented cell medium was added. The microplate was incubated at 37 °C until the next time-point. This protocol is summarized in **Figure 11**. Four samples per condition were used and the data were normalized using the negative control as a reference. The results are expressed in relative fluorescence units (RFU).

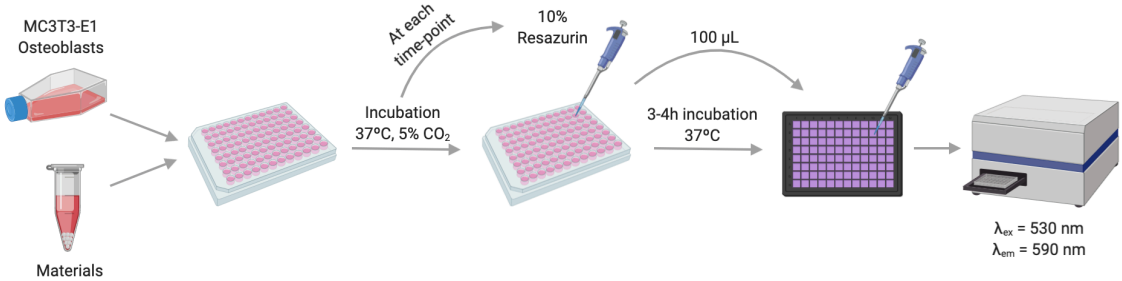


Figure 11 – Schematic illustration of the main steps implemented in the resazurin assay.

2.6. Statistical analysis

Experimental data were analyzed using GraphPad Prism Software version 6.0. Results are presented as mean values ± standard deviation (SD). The one-way analysis of variance (ANOVA) followed by the post hoc Tukey's multiple comparison test was performed and the data was considered to be significantly different when $p < 0.05$ was obtained.

3. Results and Discussion

3.1. Surface morphology characterization

SEM microscopy was used to characterize the surface morphology of the different test materials **(Figure 12)**. In **Figure 12a)** it is shown the spherical shape of the material with a mean size between 0.5 – 1 mm, which is in agreement with the information provided by the company and with Coelho et al. (2019) publication. This size range is within the range of previous results including commercial granular products, that have shown that granules with diameters of 0.1 – 1 mm allow high levels of bone regeneration (Barbeck et al., 2015; Coathup, Cai, Campion, Buckland, & Blunn, 2013). **Figure 12b)** enables the visualization of the spherical microaggregates of HAp nanoparticles, where it is expected the incorporation of MgO nanoparticles in the 3 wt% MgO materials.

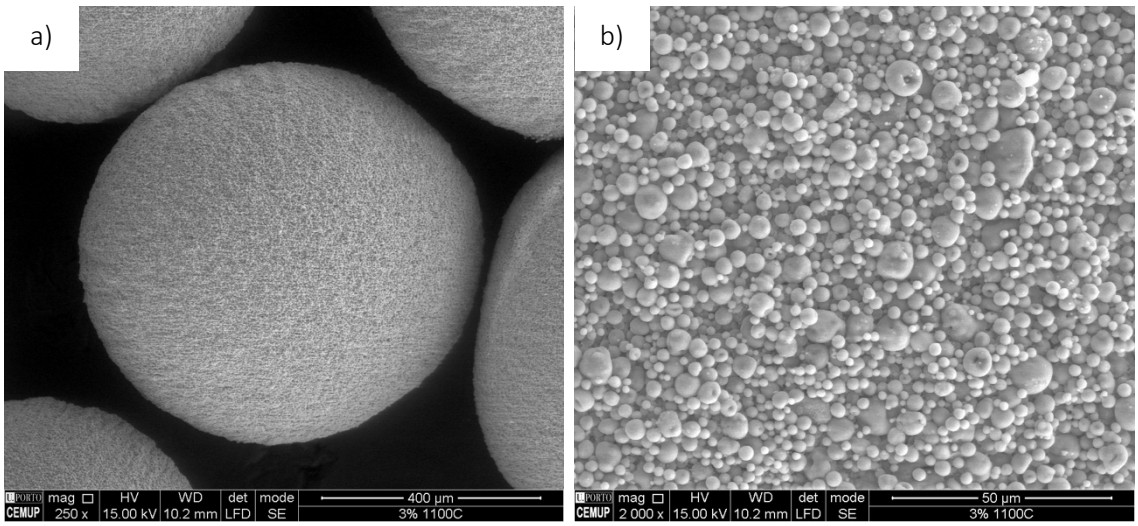


Figure 12 - SEM images of the HAp/MgO granules at low magnifications, representative for all the materials used in this dissertation a) 250x magnification allows the visualization of the spherical shape and size, and b) 2000x magnification evidences the spherical microaggregates of HAp in the surface of each granule. The sample used was the 3 wt% MgO 1100 °C.

Table 2 gathers the SEM images of the different materials used according to their sintering temperature (900 °C, 1100 °C and 1300 °C) and composition (0 wt% MgO and 3 wt% MgO), under two different magnifications (10000x and 40000x) to better visualize the resulting morphology changes. The sintering process normally occurs in the last steps of the ceramics processing, at high temperatures, in order to consolidate the shaped forms. Thus, having a positive influence on the morphology of the materials. In this step, the gases removal allows the powder to densify, increasing the grain size and, consequently, causing the shrinkage of the material (S. V. Dorozhkin, 2013).

Analyzing the images presented in **Table 2**, it is possible to confirm in the 3 wt% MgO materials the presence of the MgO nanoparticles embedded between the HAp particles or at the surface of those particles, as pointed by the black arrows in the SEM images. The EDS analysis performed in one of the spheres with 3 wt% MgO confirmed the presence of the metal oxide, containing in their elemental composition magnesium (Mg) and oxygen (O) in an atomic ratio close to 1:1 **(Figure 13b)**.

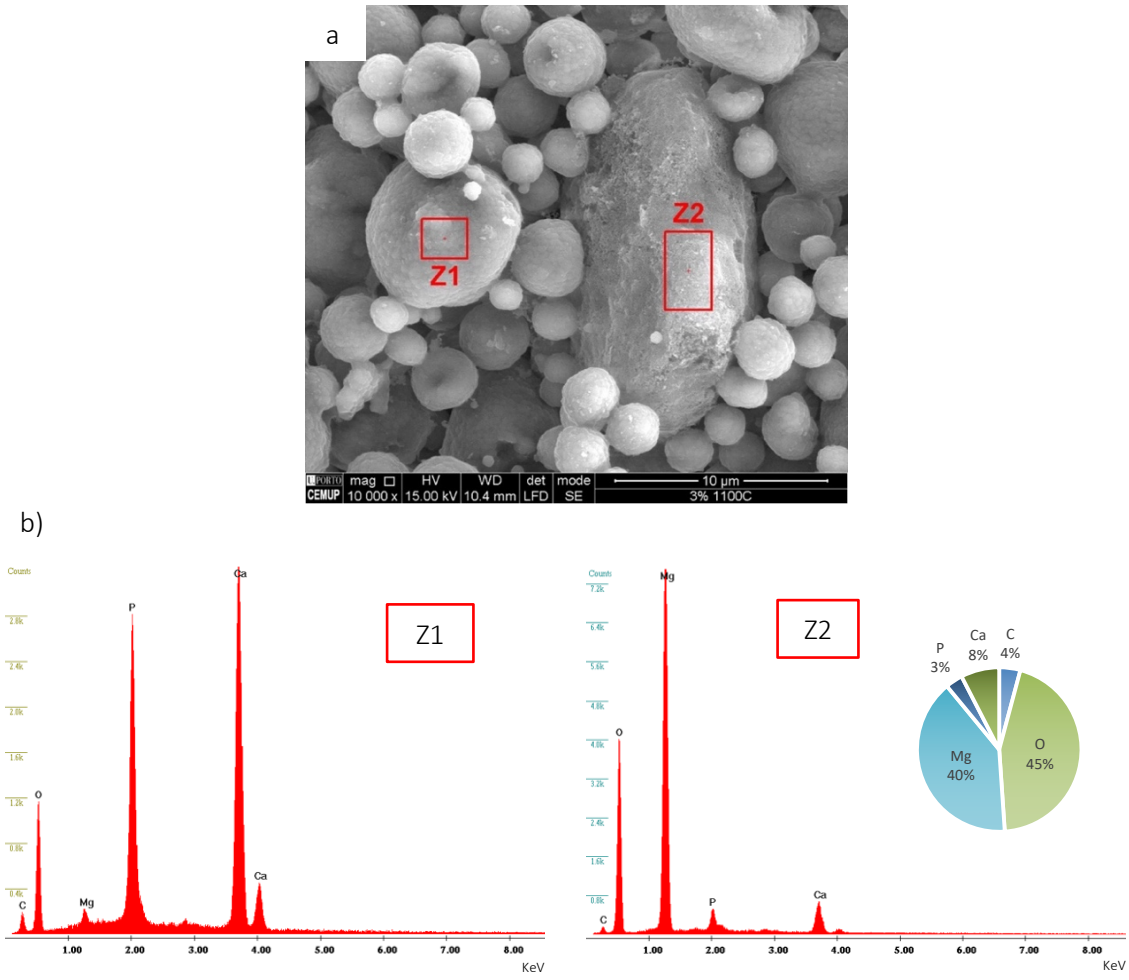
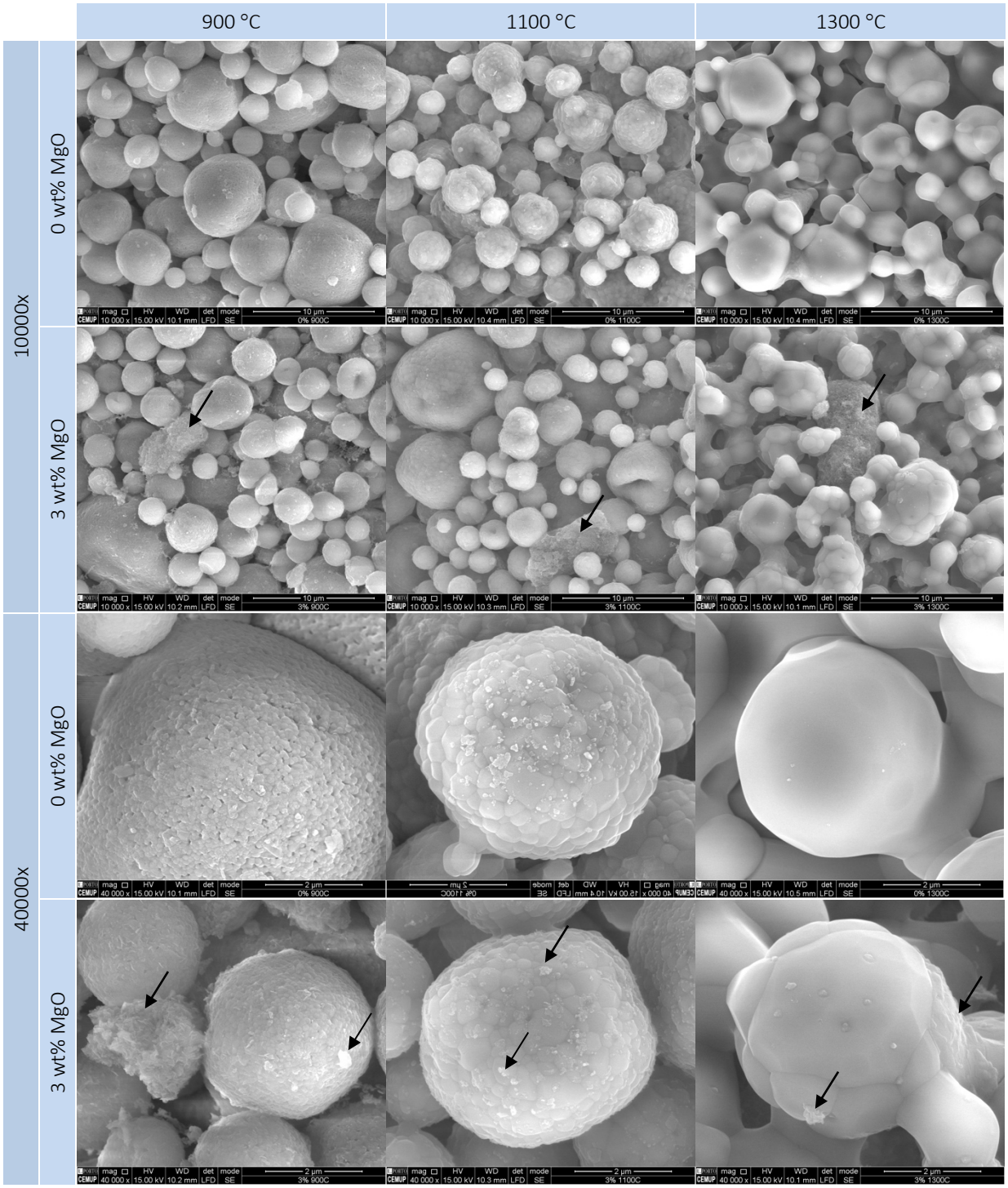


Figure 13 - EDS analysis. a) SEM image of a detailed zone in the 3 wt% MgO 1100 °C sample at 10000x magnification with two distinct zones highlighted in red, one corresponding to HAp (Z1) and other to magnesium oxide (Z2) as proved by b) the EDS spectrum.

Table 2 - SEM images of the HAp/MgO materials used in the study at high magnifications (10000x and 40000x). Surface morphology changes with the incorporation of MgO and also with the sintering temperature applied in the fabrication process. It is possible to observe MgO aggregates in the middle of HAp particles and also MgO nanoparticles on the surface of the HAp (black arrows).



Regarding the differences caused by the sintering temperature, it is well known that increasing the sintering temperature increases the resistance of the material. On the other hand, it decreases the nanostructured features, which might be desirable depending on the application of the material. Also, the higher the sintering temperature, the smoother the surface of the material. This feature, along with the loss of the nanostructure when raising the sintering temperature from 900 °C to 1300 °C, can be visualized by the SEM images in **Table 2**, for both 0 and 3 wt% MgO granular samples.

Likewise, the grain size of the spherical microaggregates of HAp is slightly higher in the sintering temperature of 1300 °C. At this temperature, it was produced a smoother and less porous material. The magnesium oxide is also affected by the sintering temperature, being more difficult to observe its incorporation in the material at higher sintering temperatures (1300 °C).

These results are in agreement with the literature, where the densification process is promoted by higher temperatures (Champion, 2013; Yeong, Wang, & Ng, 2001). Yeong et al. (2001) investigated the density of HAp, derived from powder, as a function of sintering temperature in a range of 900 – 1300 °C. They have shown that the density increases when the sintering temperature was raised from 900 °C to 1200 °C, reaching the maximum theoretical density at this temperature. Increasing the sintering temperature to 1300 °C resulted in a slightly fall in the density, which was explained by the partial decomposition of HAp over 1200 °C. Through the SEM micrographs presented in their report, it was possible to observe the densification of the structure when increasing sintering temperatures, as well as an increase in the average grain size, where the densification begins when the temperature threshold of 1000 – 1100 °C is surpassed.

3.2. Degradation tests and magnesium release from the biocomposite

Degradation tests were performed by immersion of the MgO/HAp samples in the Tris-HCl or SBF solution at 37 °C for 1, 3, 7, 14, 21 and 28 days to further investigate the degradation mechanism, to calculate the rate of weight loss of MgO/HAp granules and also the concentration of magnesium released. The obtained results are summarized in **Figure 14** and **Figure 15**.

Both tested solutions, Tris-HCl (ISO simulation test) and SBF, were freshly prepared and it was expected to simulate a physiological pH, since they were prepared with a final pH of approximately 7.4. Besides that, SBF contains an ion concentration equal to those of human blood plasma, which makes this solution even more closed to the *in vivo* environment (Kokubo & Takadama, 2006).

Regarding the weight loss results on both tested solutions **(Figure 14),** when comparing only the sintering temperatures of the granules, there were no statistical significant differences in the values between the different materials. Except on day 28, where the materials containing 3 wt% MgO have shown a significant difference between the sintering temperature of 900 °C and those of 1100 °C and 1300 °C. The degradation profile along the different sintering temperatures was 900 °C > 1100 °C > 1300 °C.

On the other hand, when comparing the materials with 0 wt% MgO and with 3 wt% MgO, there was an increase in weight loss that became more significant over time, especially from day 14, indicating that materials containing MgO in their composition degrade faster than those that do

not. These weight losses may be due to magnesium (Mg) release from the spherical granules and/or due to apatite degradation itself, which can be more elucidated through ICP and SEM analysis.

Comparing the differences between the solutions tested (Tris-HCl and SBF), the weight loss rate was clearly lower in the SBF solution **(Figure 14b))** than in Tris-HCl **(Figure 14a))**, with the weight loss percentage values in SBF after 28 days of immersion not exceeding the ones in Tris-HCl after 14 days. A slower release in the magnesium oxide and/or an apatite formation in the surface of the materials could be a possible explanation, due to the presence of phosphate and calcium ions in the SBF solution which might somehow balance with the degradation process.

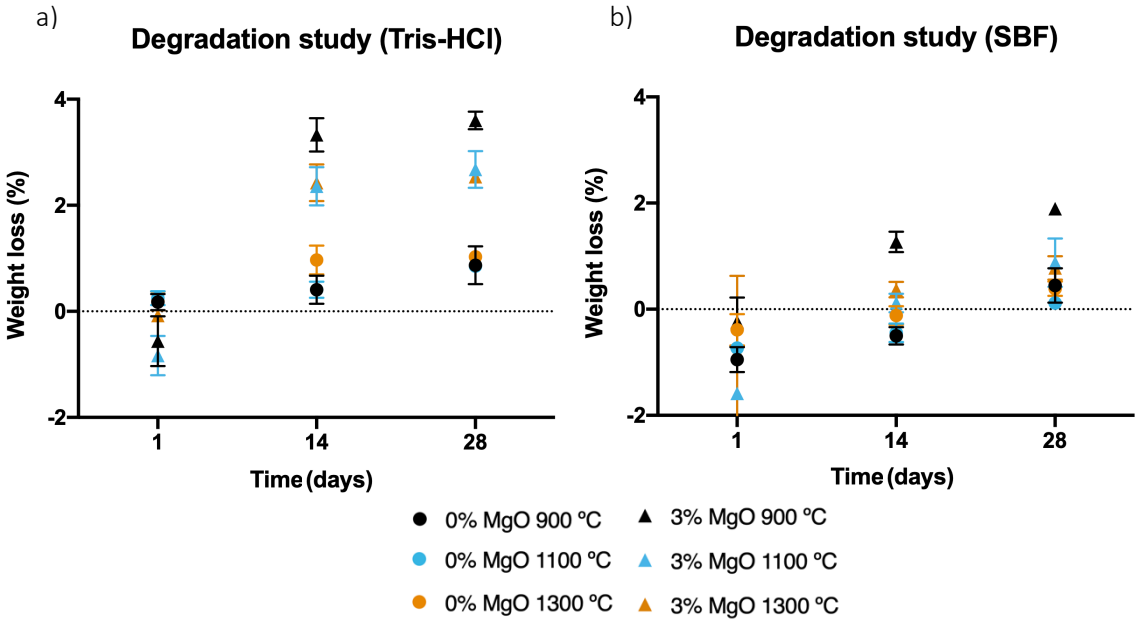


Figure 14 - Weight loss % results of the HAp/MgO samples in a) Tris-HCl solution and b) SBF solution during three time-points (day 1, 14 and 28). Results are expressed as the mean ± SD and the experiment was performed in triplicate.

In order to clarify these degradation losses, ICP-MS analysis was conducted in the supernatant solutions collected at each time point to quantify the amount of released magnesium (Mg) from the 3 wt% MgO materials when immersed in Tris-HCl or SBF **(Figure 15)**. Mg concentration was also analyzed in the 0 wt% MgO samples at day 1 and 28, and it was confirmed its absence or residual content (data not shown). Another important reason to measure the concentration of Mg^{2+} ions is their relevance in several cellular and bacterial processes (Wetteland et al., 2016).

Considering the results presented in **Figure 15**, the lower the sintering temperature, the greater the release of magnesium from the materials for both solutions (Mg release profile from HAp: 3 wt% MgO 900 °C > 3 wt% MgO 1100 °C > 3 wt% MgO 1300 °C). Once again, the results were lower in the SBF solution, with the Mg concentration values in SBF not surpassing the values in the Tris-HCl solution, at days 28 and 7, respectively. That said, the SBF has shown a more sustained release of magnesium oxide, which can be further verified through SEM analysis at different time-points. All this is in accordance with the weight loss results previously presented **(Figure 14)**. Another feature that stood out in the SBF results, was the fact that the material with a sintering temperature of 1300 °C displayed a different pattern in the magnesium release when

compared to other temperatures, presenting a low amount of this ion released, which might be due to their high density.

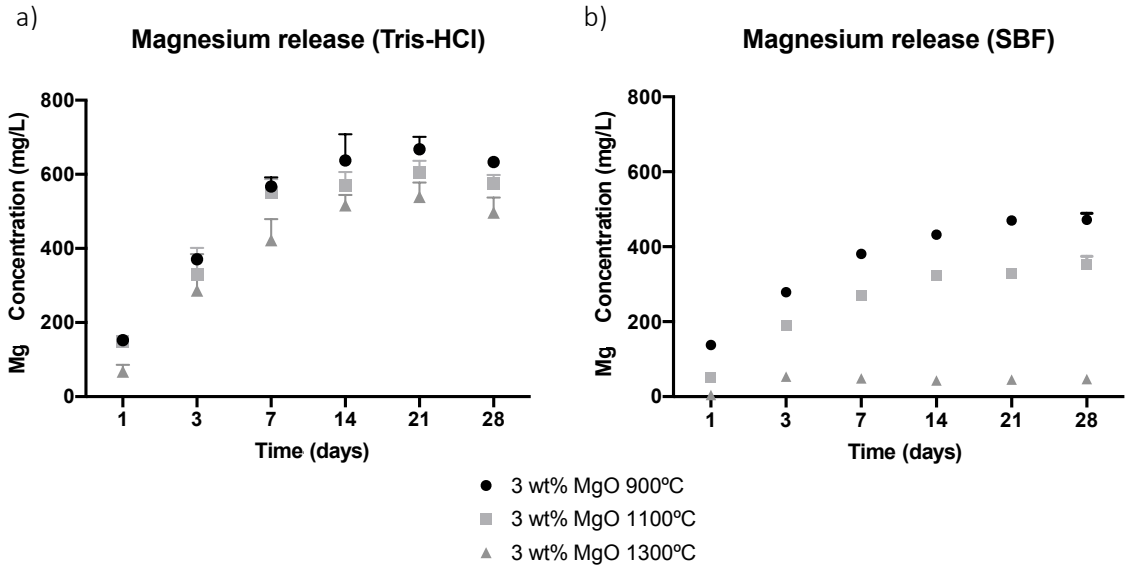


Figure 15 - ICP-MS analysis of the HAp/MgO granules in a) Tris-HCl solution and b) SBF solution during all time-points of the experience. For the values presented in b) the concentration of magnesium derived from the magnesium chloride hexahydrate ($MgCl_2 \cdot 6H_2O$) in the SBF solution was taking in consideration (Demonstration in Annex A.1). Each data point represents the mean ± SD and the experiment was performed in triplicate.

With both of these data (weight loss % and Mg concentration), and to better correlate the degradation mechanism with the magnesium oxide release, it was possible to estimate the weight percentage of MgO that was released from the materials containing this metal oxide during the different time-points of the study (Figure 16 and Annex A).

The values obtained state that the MgO released from the materials was higher in the Tris-HCl solution, with approximately half or more of its amount being released already after 7 days of immersion, while in the SBF solution the same was achieved only in the 3 wt% MgO 900 °C materials from 14 days of the experiment. The maximum amount of MgO released was obtained in the materials sintered at 900 °C that were immersed in Tris-HCl for 21 days, reaching an average of almost 75% of its initial amount. The small release of magnesium oxide from the 3 wt% MgO 1300 °C granules was also evidenced with a distinct tendency from the others, showing a little burst release from day 3 and then stabilizing for the other time-points, as observed before.

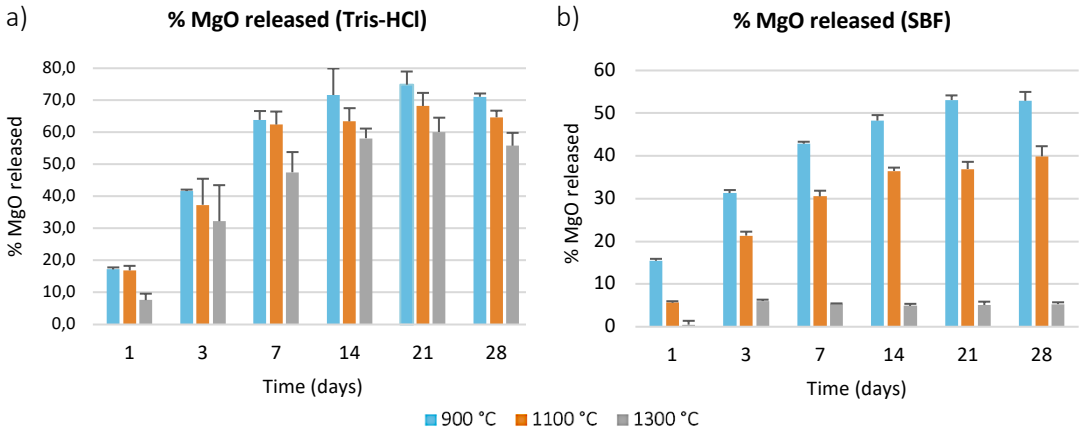


Figure 16 - Weight percentage equivalent to the magnesium oxide content released from the 3 wt% MgO granules during the degradation tests in a) Tris-HCl solution and b) SBF solution. The values are expressed as the mean percentage ± SD. An example of the calculations performed, and the values obtained are presented in the Annex A.2.

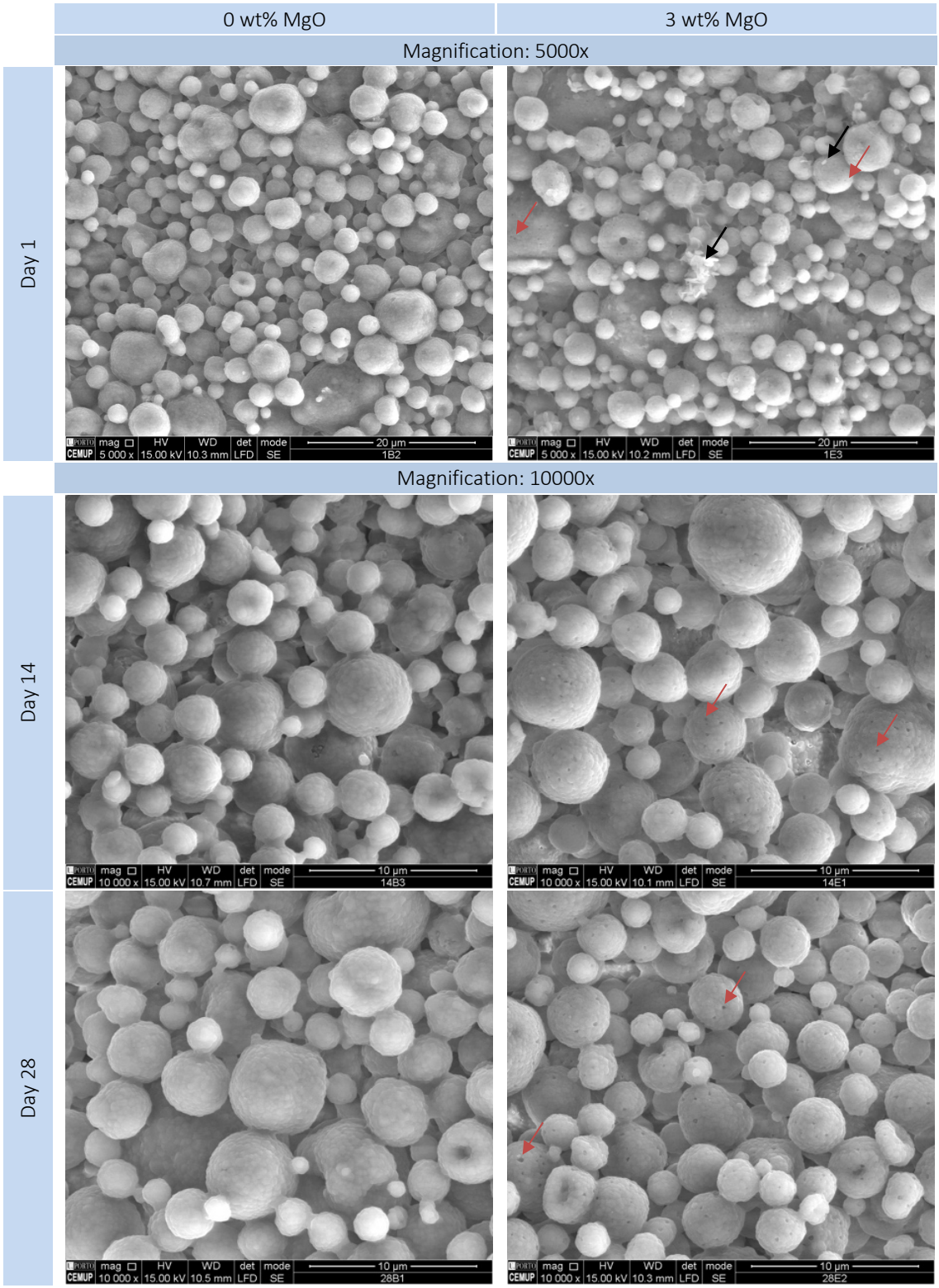
Observing the results in **Figure 16** and **Figure 15**, it might be suggested the achievement of a MgO release plateau between 21 and 28 days of immersion, especially for the Tris-HCl solution, since there was a slight decrease in the values presented in the respective time-points. Perhaps for those materials, the maximum possible amount of MgO release had already been reached at 21 days of immersion in Tris-HCl. To clarify this, a longer degradation study should be performed to see if the MgO continues to be released, or if it has actually reached a maximum plateau.

Gathering these results, it is evident that the material that degraded faster, releasing more MgO and consequently more magnesium was the 3 wt% MgO 900 °C granules, as expected. Lower sintering temperature represents higher porosity and less density of the material, leading to a higher magnesium release and subsequently higher degradation rate. In addition, Tris-HCl solution induced greater magnesium release and weight losses than SBF which is in agreement with the literature. Liu et al. (2019) reported that the presence of Tris-HCl promoted the dissolution of magnesium and that the SBF solution delayed the degradation rate and retarded the dissolution process possibly due to the inorganic ions present in the buffer.

To further evaluate the degradation process and the changes in the surface morphology, SEM analysis was carried out on magnesium oxide-containing materials sintered at 1100 °C, for 1, 14 and 28 days of the experiment. The SEM images of materials after immersion in Tris-HCl are presented in **Table 3** and the SEM images of the materials that were immersed in SBF are organized in **Table 4**.

In the degradation test performed in Tris-HCl, at day 1 it was possible to observe some areas in the spherical granules with magnesium oxide particles at the surface of the HAp nanoparticles and others where it had already been released leaving small cavities at the surface of HAp (represented by the red arrows in **Table 3**). This suggests that, prior to the release of MgO, it approximates to the surface of HAp, being afterward released. In the middle and at the end of the immersion study (day 14 and 28), the SEM images showed similar surface morphologies, and none MgO particles were visualized, indicating that all or almost all of the metal oxide present in the samples had been released. All of these is in agreement with the previous results in the solution addressed (Tris-HCl) (**Figure 15a)** and **Figure 16a)**).

Table 3 – SEM images of the 3 wt% MgO 1100 °C samples immersed in Tris-HCl at three different time-points (day 1, 14 and 28). The MgO particles are represented with black arrows and the cavities presumed to be left by these particles highlighted by red arrows.



Evaluating the SEM images of the materials that were immersed in SBF **(Table 4)**, the presence of MgO particles was observed in all the time-points presented (black arrows), contrary to what happened in the Tris-HCl assay. Also, it demonstrates a tendency for the MgO to decrease with

time, along with an increase in the number of small holes left by them (red arrows). The presence of the magnesium oxide on the hydroxyapatite surface was confirmed by the EDS analysis performed on the samples collected on day 1 **(Figure 17)**.

Once more it was verified the magnesium oxide release overtime and emphasized its migration to the surface of the HAp nanoparticles before its release. This is again in line with the weight loss and the magnesium release results.

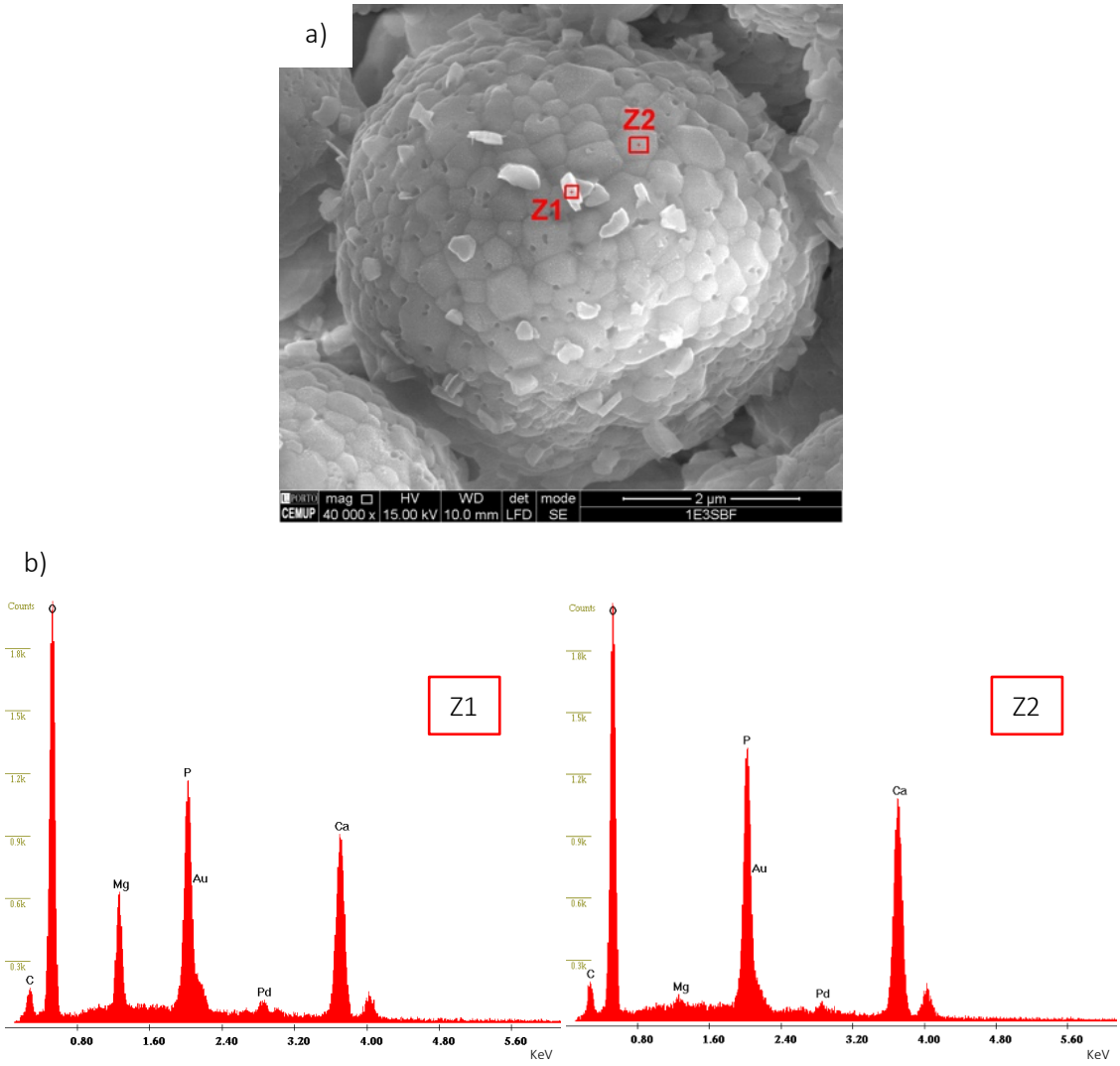
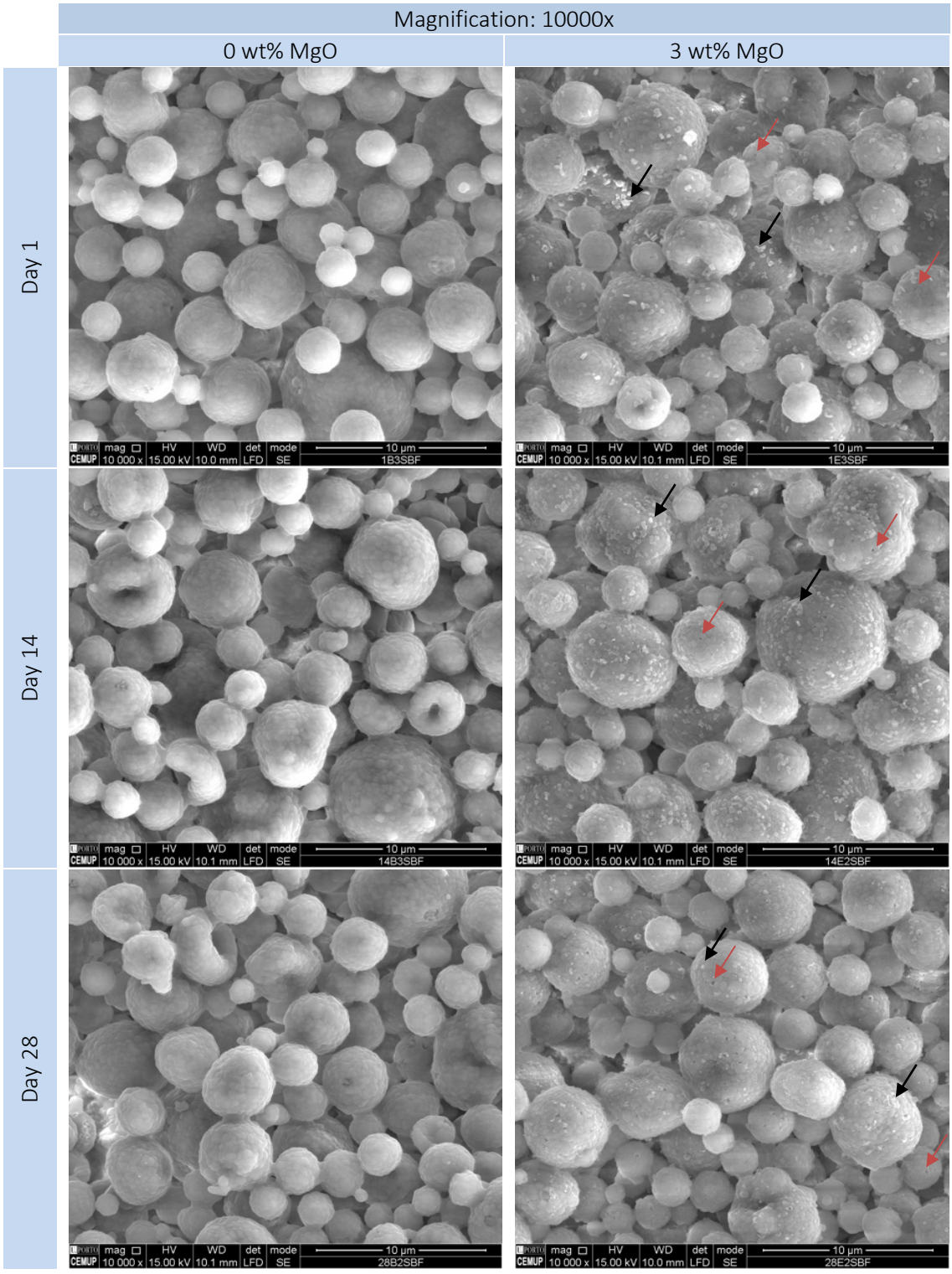


Figure 17 – EDS analysis of the 3 wt% MgO 1100 °C samples after 1-day immersion in SBF. a) SEM image of a HAp nanoparticle at 40000x magnification where it visible the magnesium oxide particles reaching the surface and the depressions left by them. b) EDS spectrum of the two highlighted zones in the SEM image indicates the existence of oxygen and magnesium, confirming the presence of MgO at the surface of the nanoparticle (Z1).

The other possible explanation, initially proposed for the lower values presented in the two previously explored results (weight loss and magnesium release), was the precipitation of HAp, which if it had occurred it should be possible to perceive in the SEM images. However, the manifestation of this process was not detected in any of the images presented in **Table 4**.

Table 4 - SEM images of the 3 wt% MgO 1100 °C samples after 1, 14 and 28 of immersion in SBF solution. As before, the black arrows indicate the particles of MgO and the red arrows the cavities after their release.



It is known that examination of apatite formation on the surfaces of ceramic materials in SBF, could predict the *in vivo* bone bioactivity of a material. Sakai et al. (2016) had shown that materials able to have apatite formed on its surface in SBF, which includes sintered HAp, could bond to living bone through an apatite layer *in vivo*, as long as the material did not induce any cytotoxic effect. These authors suggested that SEM observations should be complemented with XRD measurements since the SEM analysis could detect the material formation on a material without recognizing whether it is apatite or not, while the XRD measurement can clearly identify the apatite formation on the specimen. Their results indicated that 8 weeks post-implantation of HAp in rat abdominal subcutaneous pouches, any substantial changes were shown in the HAp structure. This was also observed throughout the degradation experiment for the pure-HAp granules (0 wt% MgO) in both tested solutions, as supported by the SEM images in Table 3 and Table 4.

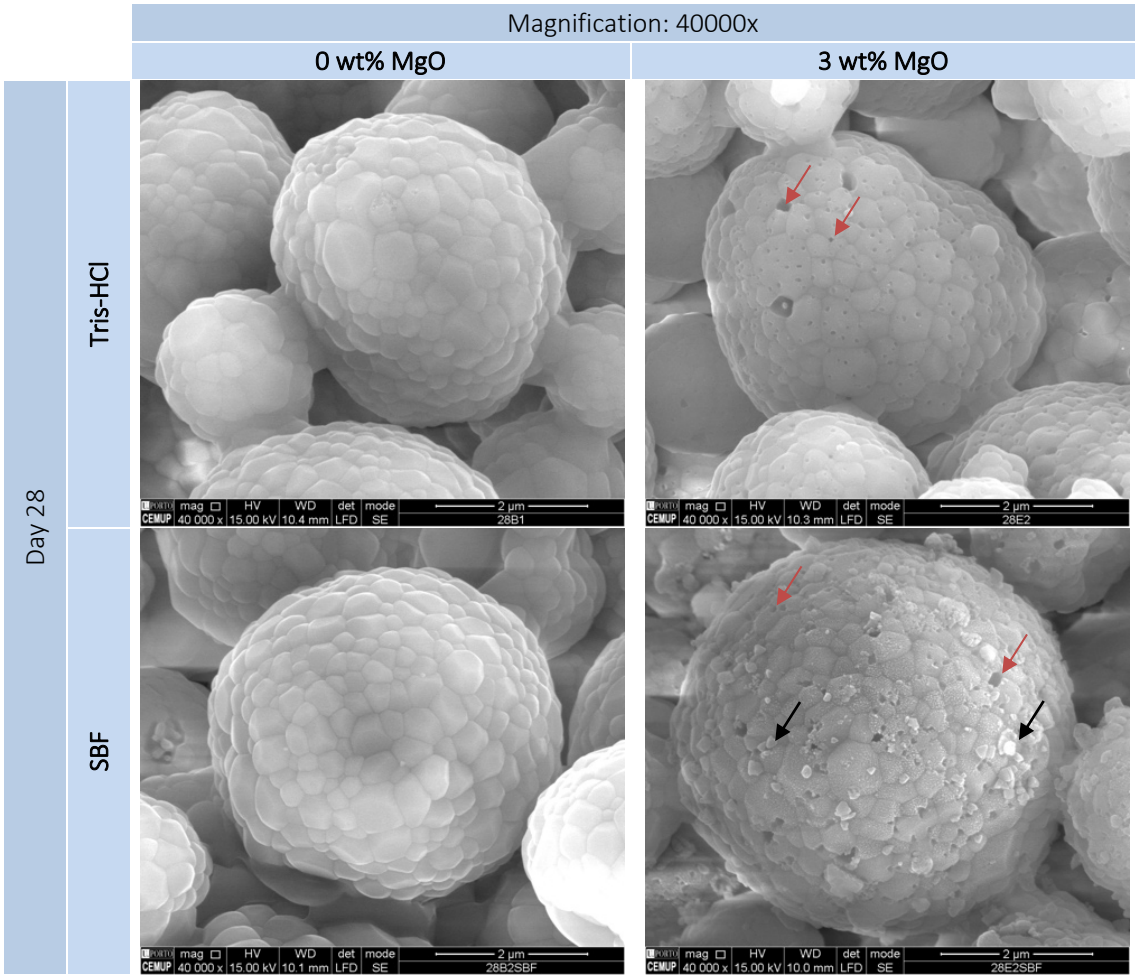
In order to better foresee the differences caused on samples by the solutions used for the degradation study after 28 days of immersion, SEM images at higher magnification were organized in Table 5.

Comparing the SBF and Tris-HCl immersed samples, it is clear the difference in morphological structure in the granules containing magnesium oxide. In the ISO test samples, no magnesium oxide was detected but only the cavities believed to be left by the release of the metal oxide. And in the SBF test it was observed some magnesium eruptions, suggesting a possible chemical reaction in the HAp surface.

In the samples immersed in SBF, it was still possible to observe, at the end of the assay, some MgO along with the depressions in the places where they had already been released, suggesting that the magnesium oxide migration to the surface was more prolonged (or sustained) than in the Tris-HCl solution. These are in agreement with the magnesium release profiles previously presented in Figure 15 and the weight loss percentage of MgO calculated (Figure 16), where the Tris-HCl promoted the magnesium release and the SBF delayed this mechanism.

In the materials used in the Tris-HCl test, it was not visible any precipitation products on their surface, whereas, in the SBF immersed samples if somehow some precipitation occurred it might be confused with the MgO particles at the surface of the HAp nanoparticles.

Table 5 – SEM images at high magnification (40000x) of the HAp/MgO spherical granules sintered at 1100 °C at the end of the immersion tests in Tris-HCl and SBF. The black arrows pointed out the magnesium oxide and the red arrows the depressions left by those.



Considering all the SEM images presented for the degradation study, it was possible to conclude that the pure-HAp materials did not show any substantial differences in the morphology upon 28 days immersion. Besides that, the incorporation of magnesium oxide in the granules occurred by means of physical adhesion since it degrades faster than HAp, with the major MgO loss through the grain boundaries of the HAp nanoparticles. The mechanism of its release was believed to be through migration to the surface and then dissociation, occurring faster when the Tris-HCl buffer was used.

Taking together these results, the main highpoints are that materials with magnesium oxide and produced at lower sintering temperatures, displayed higher weight loss rates **(Figure 14)** that could be related to the greater MgO release **(Figure 16)**. This suggests that the 3 wt% MgO composites degraded primarily through the release of the metal oxide.

Also, concerning the different buffers tested, the Tris-HCl has shown to be more advantageous in the degradation and MgO release from the granules, probably due to the absence of high concentrations of ions involved in apatite formation, which are present in the SBF. According to the literature, some components of the SBF solution have been proved to contribute to the lower degradation rate verified, with the calcium chloride ($CaCl_2$) having the major role. Upon its

presence, the degradation rates were shown to decrease by the development of apatite precipitation, proposed to function as a surface protecting deposition. Sodium hydrogen carbonate ($NaHCO_3$) in co-addition with $CaCl_2$ was proved to enhance the formation of $MgCO_3$ and apatite formation (Agha et al., 2016).

It is known that the degradation rates of a material depend on their chemical compositions, crystallinity, and physical forms, such as porosity, pore size and distribution, and grain size. Also, in materials made from powders, the degradation is predominantly controlled by the disintegration of particles (Hench & Best, 2013).

These *in vitro* immersion experiments, in Tris-HCl and SBF solutions, provided an indication of the biodegradation behavior of the biocomposite granules during the *in vivo* implantation. They have shown that the degradation rate is influenced by the simulated buffer solution, as reported by Gonzalez, Hou, Nidadavolu, Willumeit-Romer, and Feyerabend (2018). Since most of the times an immediate Mg release upon implantation in the organism is a desirable effect, Tris-HCl buffered SBF solution was previously recommended for *in vitro* evaluation (Liu et al., 2019).

3.3. *In vitro* microbiological assays

The antibacterial properties of the HAp/MgO granules were tested against a common pathogen associated with implant infections, *S. aureus*, and the effect of the different materials on the bacteria growth is presented in **Figure 18**.

When HAp/MgO granules were incubated with *S. aureus* for 24 h, a significant reduction of bacteria growth for the 3 wt% MgO composites was observed when compared with pure HAp samples (0 wt% MgO), despite the sintering temperature of the materials. This highlight the antibacterial properties of magnesium oxide since its addition significantly reduces the number of planktonic bacteria.

Granules with 3 wt% MgO produced under a sintering temperature of 900 °C, have shown higher growth inhibition, with a 99.99% reduction in the number of microorganisms. This was expected because these materials release magnesium faster than the others, as proved by the degradation studies. Since MgO is the component that confers the antimicrobial activity to these materials, a higher concentration of magnesium in the medium represents higher antibacterial potential and consequently more inhibition of *S. aureus* growth. That is in conformity with the literature, where the use of MgO powder had shown antibacterial effects towards *S. aureus* (Coelho et al., 2019; Jun Sawai et al., 2000).

Nguyen et al. (2018) investigated the concentration effects of magnesium oxide nanoparticles (nMgO) against prevalent infectious bacteria, including the Gram-positive bacteria *S. aureus*, and reported that bacterial viability was dependent on the nMgO concentrations. They evidenced that the lowest concentration required to inhibit the visible growth of *S. aureus* was 0.7 mg/mL and that the CFU of *S. aureus* had reached the lowest at 1.4 mg/mL of nMgO, showing a death rate of greater than 99.99% (less than 0.01% of bacteria was viable).

Another important finding was that the bacteria strain influences the evaluation of the antibacterial potential of a material, possibly due to the different physicochemical characteristics.

This was found since the same 900 °C sintered materials and experimental conditions were used as the ones investigated by Coelho et al. (2019), with the only difference being the bacterial strain, and different outcomes were obtained. On their report, total growth inhibition of *S. aureus* was observed for the 3 wt% MgO samples, whereas in the present work that was not achieved **(Figure 18)**.

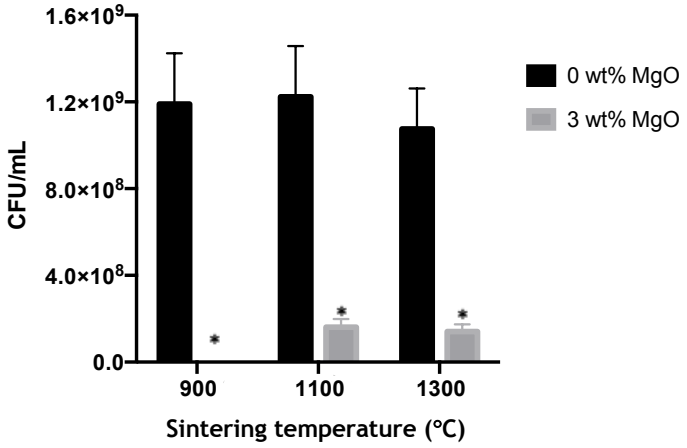


Figure 18 - Antibacterial effect of granules after 24 h incubated with *S. aureus*. Population of planktonic bacteria results are expressed in CFU/mL and * represents a significant reduction between the pure HAp granules (0 wt% MgO) and the 3 wt% MgO granules ($p < 0.05$). Each data point represents the mean ± SD of 3 independent experiments performed in triplicate (n = 3).

Summarizing, the granular biomaterials studied have shown to be effective at reducing bacterial activity *in vitro* when a 3 wt% MgO is present in their composition, regardless of the sintering temperature. A possible explanation for the decrease in the bacterial growth with the presence of MgO is the formation of superoxide ions or other reactive oxygen species (ROS) at the surface of the material, due to the easy hydration of MgO to $Mg(OH)_2$ (chemical reaction below). This hypothesis will be further elucidated in the document.

$$Mg + 2H_2O \rightarrow Mg^{2+} + 2OH^- + H_2 \qquad (2)$$

Regarding the initial bacterial adhesion test, a higher bacterial density than before was used to overlay the material's surface with bacteria, in order to evaluate if changes in the surface morphology of the granules had any influence on *S. aureus* adhesion after only 1 h incubation.

As stated before, several factors can influence the initial bacterial cell attachment process including the chemical composition, surface charge, hydrophobicity, and surface roughness of the material. The materials used for this study were presumed to be negatively charged, as supported by the zeta potential results presented by Coelho et al. (2019), with the inclusion of MgO decreasing these negative charges. Concerning the surface charge of the bacteria, it differs within bacterial species but usually, the overall charge is negative, suggesting that electrostatic repulsion of similar negative charges might occur at the surface of the material.

The results obtained for the initial adhesion experiment **(Figure 19)**, indicated that neither the different sintering temperatures or the metal oxide addition had a significant effect on *S. aureus* adhesion after 1 h incubation with the materials. However, there was a slight decrease in the initial adhesion with the temperature (clearer for the pure HAp granules), and an increase with

the presence of MgO. This might be due to the higher material density with increasing sintering temperatures, mainly between 1100 °C and 1300 °C, as demonstrated before **(Table 2)**. The decrease in the granules surface roughness provided fewer contact points for bacterial adhesion, thus reducing the antimicrobial activity.

Regarding the presence of magnesium oxide in the granules, a major difference was achieved for the ones with a sintering temperature of 1300 °C, which are those that presented a smoother surface due to grains coalescence, as observed by SEM **(Table 2)**. It was expected more irregularities and consequently an increase in the materials surface roughness due to the incorporation of the MgO, thus promoting bacterial adhesion.

In addition, since the negative charge of the material slightly decreased with MgO inclusion, the electrostatic repulsion between the material surface and bacteria might be reduced, enhancing the microbial adhesion. These conclusions were made based on a review of the mechanisms of bacterial adhesion to biomaterials surfaces addressed by Katsikogianni and Missirlis (2004).

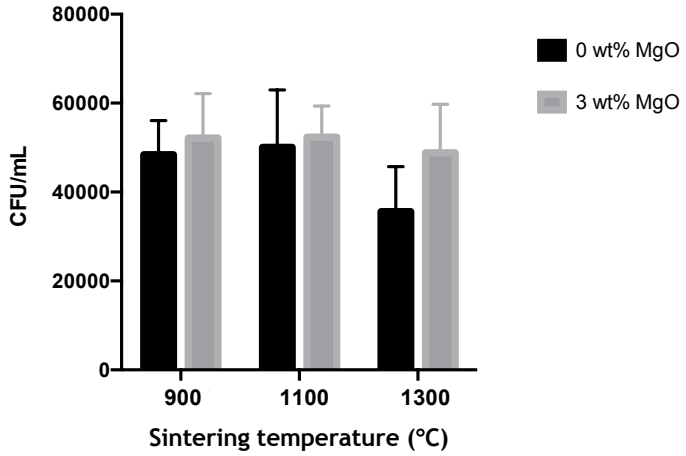


Figure 19 - Initial bacterial adhesion studies. Number of adherent bacteria cells in the materials after 1 h incubation is represented in CFU/mL. Results are expressed as mean ± SD (n=5)

Contrary to what was found in the developed experiment, for longer incubation periods (24 h for example), the presence of MgO have shown an opposite influence on bacterial adhesion, as expected. Nguyen et al. (2018) demonstrated that bacteria adhesion (including the Gram-positive bacteria in question, *S. aureus*) decreased after 24 h incubation with MgO nanoparticles in a concentration-dependent manner, supporting that the MgO has indeed antibacterial properties.

Correlating granules antibacterial effect **(Figure 18)** with the initial (1 h) bacterial adhesion **(Figure 19)**, despite a similar adhesion behavior, the presence of MgO in the materials induced growth inhibition of the bacteria. Having different outcomes depending on the sintering temperature of the material, since the degradation and MgO release was different, as previously proven in section 3.2. All this emphasizes the antibacterial potential of MgO, exhibiting a decrease of adhesion with time and a consequently inhibition of biofilm formation.

Relatively to the mechanism of antibacterial action of the magnesium oxide, many theories have been proposed and demonstrated over the years (Leung et al., 2014; Nguyen et al., 2018; Jun Sawai et al., 2000), however, the exact mode of action is not defined yet.

In this work, the mechanism explored was the production of reactive oxygen species (ROS), which is one of the leading theories for the antimicrobial action of MgO. It is believed that oxidation/reduction reactions could occur at the MgO surface, generating ROS species like superoxide radical (O_2^-), hydrogen peroxide (H_2O_2), and hydroxyl radical ($^{\bullet}OH$), which might induce a chemical attack to the bacterial cell wall and eventually lead to lethal damage.

ROS detection strongly depends on the method sensitivity and specificity of the probe. Therefore, $DCFH_2$-DA probe was used due to higher sensitivity of fluorometric assays, and also the fact that it has been widely applied as fluorescence probe for generalized oxidative stress (Chen et al., 2010).

From the results previously obtained, the materials that were sintered at 1100 °C showed to be more advantageous in terms of balance between degradation and antibacterial potential. Considering these data, the materials chosen for this microbiological assay were the ones sintered at 1100 °C.

As mentioned in the section 2.4.4, two different start points were used to detect the ROS species, the $DCFH_2$-DA and the $DCFH_2$ compound. This was made because the ROS species does not directly interact with $DCFH_2$-DA but with its hydrophilic derivative ($DCFH_2$), which requires esterases for the $DCFH_2$-DA hydrolysis **(Figure 10)**. The higher resistance to oxidation verified by the $DCFH_2$-DA over its derivative product, $DCFH_2$, was justified by the absence of the easily oxidizable phenol moieties in the $DCFH_2$-DA (Bonini, Rota, Tomasi, & Mason, 2006).

Since esterases will not be present in the bacterial-free study, and also the bacteria might have low esterase activity, the $DCFH_2$ was chemically produced by the cleavage of $DCFH_2$-DA with NaOH and used for ROS detection. TBHP mimics ROS activity to oxidize $DCFH_2$-DA to fluorescent DCF, being used as a positive control for the ROS generation. The results obtained are displayed in **Figure 20** and **Figure 21.**

In **Figure 20** it is possible to see the effect of cells loaded with $DCFH_2$-DA vs $DCFH_2$, and the differences in ROS production between materials containing or not MgO. The level of $DFCH_2$-DA or $DCFH_2$ oxidation by bacterial cells incubated with 3 wt% MgO granules was significantly higher than bacteria incubated with pure-HAp granules or without any materials. That is, for both protocols, generation of ROS was only observed in *S. aureus* cells treated with 3 wt% MgO. As for the materials with 0 wt% MgO, the values acquired were similar to those of negative control (bacteria in TSB). These results suggest that the 0 wt% MgO material, did not induced any oxidative stress in the bacteria.

Comparing the two materials (0 wt% MgO and 3 wt% MgO), it is quite clear the difference in their oxidation potential, visible through the variation of fluorescence values obtained **(Figure 20)**. The differences in the RFU values between $DCFH_2$-DA and $DCFH_2$ might be due to a low esterase activity of *S. aureus* or by the easily oxidation of the $DCFH_2$ (as previously mentioned), since many other enzymes can play the role of esterases and therefore producing the $DCFH_2$ at high extent.

All living organisms produce enzymes to defend themselves against ROS. The bacteria tested in this study can produce superoxide dismutase (SOD), a cellular antioxidant defense enzyme that might act on the O_2^- and form H_2O_2. Then, it is neutralized to H_2O and O_2 by another antioxidant

enzyme produced by *S. aureus*, named catalase (Karavolos et al., 2003). Given that, these bacterial cells should exhibit a low level of fluorescence as verified by the negative control data (Figure 20).

ROS generation in cells might occur through extracellular (exogenous) and intracellular (endogenous) mechanisms (Choi & Hu, 2008). Materials with 3 wt% MgO suggested factors other than intracellular ROS, once they appeared to be more toxic than the pure HAp samples. There are high probabilities that the presence of MgO interferes with the $DCFH_2$ and its diacetate form ($DCFH_2$-DA), producing more reactive species that will lead to a higher fluorescence in this samples.

ROS only increased significantly when the bacterial cells were in contact with the 3 wt% MgO granules, emphasizing the production of reactive oxygen species as a mechanism of antibacterial action of this metal oxide, as already demonstrated by Al-Hazmi et al. (2012); Huang et al. (2005); Jun Sawai et al. (2000); Yamamoto et al. (2010).

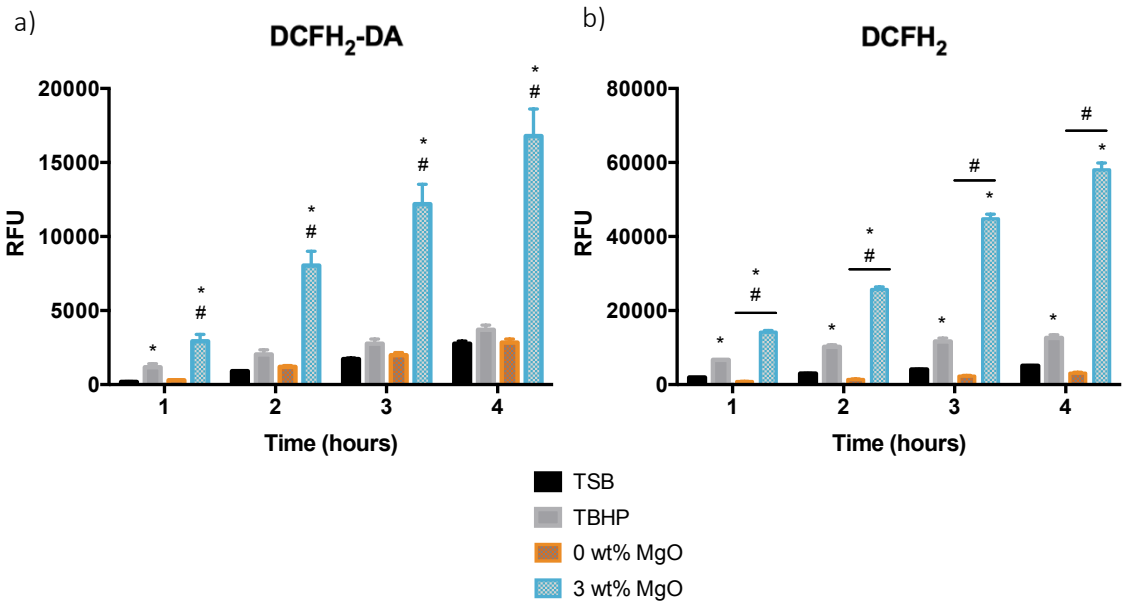


Figure 20 – ROS production by *S. aureus* bacterial cells upon 24 h incubation with the granules (G1) during 1, 2, 3 and 4 h incubation either with a) $DCFH_2$-DA or b) $DCFH_2$ (20 μM final concentration). TSB medium was used as negative control and TBHP as positive control. Results are expressed in terms of relative fluorescence units (RFU) and background fluorescence was taking into consideration. The experiment was done in triplicate. * represents a significant difference when compared with negative control, and # symbolizes a statistical difference when compared with the positive control ($p < 0.05$).

In order to understand how this material affects $DCFH_2$ fluorescence, it was compared the ROS production between the different material sizes (G1 and G2) with and without bacteria. The data was acquired after 1 h incubation since it is known that the time needed for the dye to properly perform its function (react with ROS species and exhibit fluorescence) is 45 min to 1 h incubation. (Eruslanov & Kusmartsev, 2010). The respective results are presented in Figure 21.

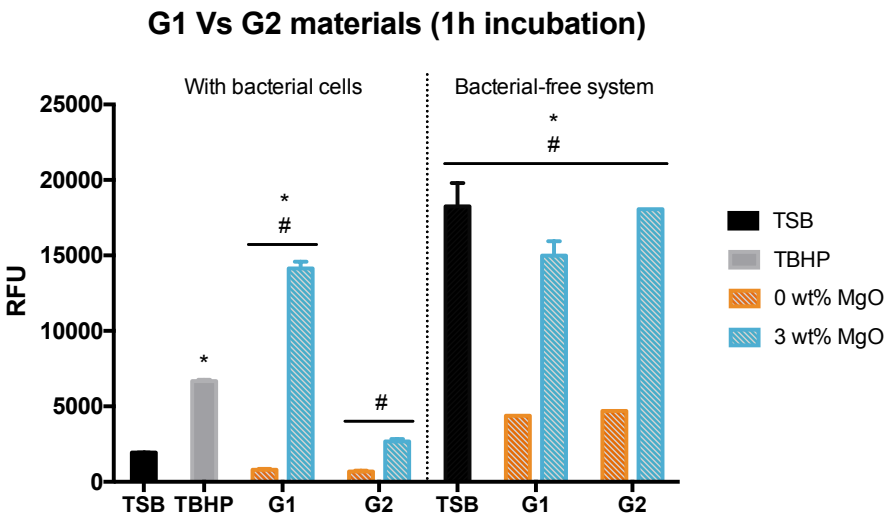


Figure 21 – $DCFH_2$ assay for the detection of ROS produced by the materials alone (bacterial-free system) or by *S. aureus* incubated with the materials for 24 h, upon 1 h incubation with 20 μM of $DCFH_2$. Both material sizes were tested (G1 and G2) and the study was performed in triplicate. Results are expressed in terms of relative fluorescence units (RFU) and corrected for background fluorescence. * represents a significant difference when compared with negative control (TSB), and # symbolizes a statistical difference when compared with the positive control (TBHP) ($p < 0.05$).

Larger size granules (G2) with the inclusion of MgO induced lower RFU values than the smaller materials (G1). That is, none of the materials with a bigger size (G2) induced the formation of exogenous ROS species, since their RFU values were significantly lower than the positive control, suggesting that the ROS effects might be size dependent. Higher material size decreases ROS production and thus the bactericidal activity, as reported by Makhluf et al. (2005). Another possible explanation is that the MgO present in the G2 materials could be neutralized by the SOD produced by bacteria since these materials probably release the MgO slower than the G1 materials. Therefore, in the G2 a lower concentration of MgO is available to act against the bacteria.

Analyzing the bacterial-free system, in the control only with the TSB medium the elevated fluorescence intensity might be attributed to the auto-oxidation of the probe, showing that the $DCFH_2$ was extensively oxidized as reported by Setsukinai, Urano, Kakinuma, Majima, and Nagano (2003). In addition, it was possible to observe a distinct difference between the 0 and 3 wt% MgO suggesting that the MgO-containing materials had the capacity to produce ROS itself as demonstrated by the increased fluorescence values, that could also reflect metal impurities in the medium.

Bacteria presence led to a reduction in the fluorescence values, which might be explained by the internalization of the probe by the bacterial cells, that will then oxidize the $DCFH_2$ in the presence of reactive species, to DCF. Thus, supporting that these RFU results are due to the DCF, which can be further related to the formation of ROS species. MgO addition increased RFU values both in the presence or absence of bacterial cells, showing the MgO influence in ROS production.

ROS generation was enhanced for the 3 wt% MgO versus 0 wt% MgO materials, particularly for the granules with a smaller size (G1). These results clearly demonstrate the generation of ROS in bacterial cells treated with the MgO-containing granules. Moreover, the extent of ROS production

was dependent on the presence of MgO, and the size of the material, that influences the MgO concentration available to act against bacteria. Not all the ROS produced could be timely neutralized by the SOD and therefore the excess ROS could cause destructive damage to the bacteria in the 3 wt% MgO granules with a size range of 0.5 - 1 mm.

3.4. *In* vitro cytocompatability test

Since the purpose of the HAp/MgO materials is their application as bone substitutes, they must present biocompatible (non-toxic) properties. It is known that biocompatibility evaluation of biocomposites strongly depends on:

- materials type;
- structural and functional characteristics;
- manufacturing process;
- sterilization techniques;
- linearity, sensitivity and reproducibility of the biocompatibility assay;

Low toxicity of resazurin makes it suitable for longer studies and follow-up assays can be performed on the same cells for different cell culture time. MC3T3-E1 cell viability was measured by resazurin assay and the results are illustrated in Figure 22.

According to literature, many researchers have shown evidences that besides the surface chemistry of a material, its topography has also an important effect in the regulation of cell behavior in terms of cell adhesion, activation, proliferation, alignment and orientation (Iqbal & Keshavarz, 2017).

For this metabolic activity assessment, both materials sizes were used (G1 and G2) and two sintering temperatures were tested, 1100 °C and 1300 °C. The irreversible reaction of resazurin to resorufin is proportional to aerobic respiration (O'Brien, Wilson, Orton, & Pognan, 2000), thus RFU values presented can be directly correlated with the MC3T3-E1 cell viability.

Exploring the results in Figure 22, cell proliferation has become more evident over the time. However, the presence of MgO decreased cell viability, what turn out to be less significant throughout the experiment.

For larger size (G2) materials sintered at 1100 °C, cell viability of pure HAp granules was always similar to the negative control (cells in TCPS). On the second time-point studied (day 7) only the materials containing MgO showed a significant difference in the cell viability when compared to the negative control (3 wt% MgO > 0% MgO > Negative control) (Figure 22b). On day 14, all the materials displayed similar cell viabilities when compared to the negative control, except for small size (G1) samples with 3 wt% MgO sintered at 1100 °C. However, it was shown an increase in cell viability compared to previous time-points (Figure 22c)).

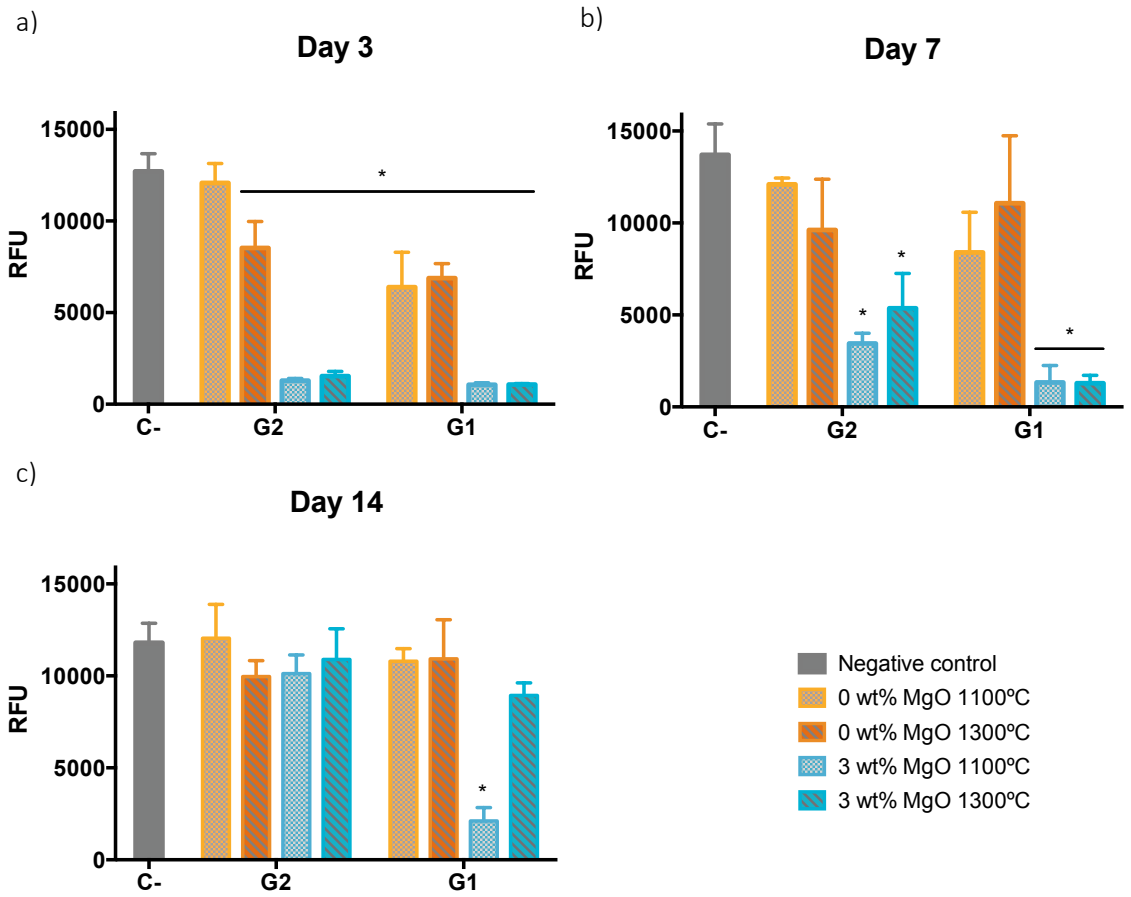


Figure 22 – Metabolic activity of the MC3T3-E1 osteoblasts seeded with the test materials at a) day 3, b) day 7 and c) day 14. Resazurin fluorescence was measured 3-4 h post-incubation. * represents significant differences compared to the negative control (TCPS).

The physical aspect of the material not only influences bacterial adhesion but also eukaryotic cells adhesion, i.e. with lower adhesion for eukaryotic cells. Larger size granules (G2) showed to be more adequate for the MC3T3-E1 cells, suggesting that the larger surface area on these granules helps in the maintenance and proliferation of cells.

Considering that the 1300 °C-sintered materials had smoother surfaces **(Table 2)**, at day 14 these materials had more cells than the materials sintered at 1100 °C **(Figure 22c))**. This could be explained by the higher cell spreading on smooth surfaces than on rough surfaces, as previously reported (Nothdurft et al., 2015).

The granular structure of these materials provides a 3D environment to the cells. Therefore, the higher metabolic activity in the negative control might be due to the 2D environment, that allows more cells to adhere and proliferate (J. R. Jones, 2006).

As already stated, ROS species could be formed on the surface of these materials, being able to trigger intracellular oxidative stress, not only for bacteria but also for mammalian cells. Mechanisms of cellular toxicity, such as elevated ROS production that exceeds the capacity of the cellular antioxidant defense system, causes cells to enter a state of oxidative stress, which results in the damage of cellular components such as lipids, proteins, and DNA (Xia et al., 2006). Since the G1 materials containing MgO were shown to produce ROS at their surface **(Figure 20)**, a

possible explanation for their higher cytotoxicity might be due to the possibility of ROS production by MC3T3 cells in the presence of these granules. Further studies to evaluate the ROS formation should be done to elucidate this.

These results demonstrate that the granules were not cytotoxic. Overall, G2 materials demonstrated to be more promising for cells proliferation, whereas the smaller size granules (G1) showed to be more aggressive to cells.

4. Conclusions and future perspectives

The development of new anti-bacterial medical devices has been proposed as a strategy to interfere in bacterial adhesion and inhibit biofilm formation, in order to prevent implant-associated infections and subsequently reduce patient morbidity and economic costs.

Many combinations of antimicrobial agents with biomaterials have been applied for that purpose, including the use of magnesium oxide. Several factors affect the material antimicrobial activity involving the contact between MgO and bacteria, bacterial cell density, bacterial strain, and lastly, the size, shape, and charge of the material.

In this dissertation, pure HAp or with 3 wt% of MgO spherical granules were characterized and their antibacterial potential was assessed against the Gram-positive bacteria *S. aureus*, that is strongly attributed to the implant-associated infections.

A loss of the nanostructure in the spherical granules for higher sintering temperatures was observed along with densification and increase in the grain size. The MgO inclusion also affected the surface topography of the HAp granules. For the degradation tests, the materials with MgO in their composition degraded faster than the ones without this metal oxide. Between the different sintering materials, the lowest (900 °C) showed a higher weight loss and magnesium release, this means that the 3 wt% MgO 900 °C granular composite presented the highest degradation rate and magnesium oxide release. However, in an ideal situation, the biodegradable implant material should be slowly resorbed and replaced by natural tissue, meaning that, higher sintering temperatures should be taken into consideration for this to happen, as the sintering temperature of 1100 °C.

The granules containing 3 wt% MgO were able to significantly reduce bacterial activity *in vitro*, regardless the sintering temperature, although this reduction was more visible for the 900 °C, with a notable decrease of CFU number.

Controlling the topography of a material is a way to influence bacterial interaction with the surface of the material, however changes in the surface morphology of the granules, as analyzed by the SEM images for the different sintering temperatures, did not have significant effect on *S. aureus* adhesion after 1 h incubation, suggesting that these modifications have more effect for longer incubation times.

The explored mechanism for the exhibited bactericidal properties of magnesium oxide was the production of reactive oxygen species. Indeed the 3 wt% MgO materials were capable to induce the formation of ROS by *S. aureus* bacteria, as supported by the increased fluorescence values upon MgO inclusion in the materials.

All the granules tested showed to promote osteoblast cell proliferation over time, being the G2 materials the ones that presented higher cell proliferation. The smaller size and MgO-containing extracts (G1) disturbed more the cell viability process, indicating that osteoblast cell response is influenced by both the composition and surface topography of the material, as well as, the size of the material. Further studies to evaluate if the granules extracts are capable of inducing ROS production by the MC3T3-E1 osteoblasts should be conducted to add more value to this biocompatibility assay.

The presence of nanostructured MgO in the HAp spherical granules provides an additional measure to minimize the risk of infection and prevent failure of the implant, since these granules were able to considerably reduce bacterial growth, apart from presenting adequate size, spherical morphology and long shelf-life. Upon implantation into the host, it is desirable an immediate MgO release, however, this process should be balanced with the degradation of the material that, as mentioned before, is more pronounced in the 900 °C sintering temperatures. For that reason, the intermediate sintering temperature tested, 1100 °C, that represents the beginning of the densification process, might be the best biomaterial for implantation procedures.

Since bacterial adhesion is a very complex process influenced by several factors, including materials surface roughness and bacterial properties, further studies are needed to clarify this bacterial-material interaction. This comprises the use of different bacterial species and strains involving Gram-positive and Gram-negative bacteria, different cell viability assays, the use of materials with different weight percentages of MgO in the different sintering temperatures tested, in order to quantify and compare concentration effects of MgO, and finally, evaluate the adhesion and morphologies of different microorganisms cultured with MgO-containing granules.

To better understand the morphological changes in the bacterial cell wall and cell membrane due to the action of MgO, SEM and atomic force microscopy (AFM) analyses should be conducted in parallel with the microbiological studies. Also, others bacterial viability assays may be carried out, including: (1) fluorescence microscopy or flow cytometry techniques with Syto 9 and propidium iodide dyes for example, which are very useful to detect cells alive (green labeled) and dead (red labeled) in relation to their membrane integrity (Berney, Hammes, Bosshard, Weilenmann, & Egli, 2007); (2) molecular methods (Keer & Birch, 2003); (3) luminometry; and (4) spectrophotometry; among others. The accuracy of these indirect methods is highly dependent on the mode of cell death and environmental conditions. Methods that allow simultaneous measurement of multiple viability parameters provide a better correlation with bacterial cell viability than dependence on any single analytical technique, making multiparameter assays more prevalent choices for various applications. An effective monitoring system for the identification of viable cells could be provided by coupling a quantitative approach with array-based detection systems to allow simultaneous analysis of multiple targets (Davis, 2014).

Regarding the ROS detection assay, the use of plate readers may present a possible problem since it measures total fluorescence and does not distinguish between intracellular and extracellular fluorescence from chemical reactions in the culture medium. Thus, an alternative procedure might be flow cytometry and/or confocal microscopy that allows to measure and visualize the intracellular fluorescence of cells in the culture media. Besides that, other ROS detection probes, as rhodamine, and other measurements techniques should be performed (H.-S. Wang, 2016).

As for the cytotoxicity study, since it is difficult to visualize the cells with the material directly in the 96-well plate by normal microscopy, other approaches can be performed to evaluate and characterize the cell viability. This includes DNA quantification, AFM, Confocal laser scanning microscopy, SEM to evaluate cells adhesion, and others (J. R. Jones, 2006). It would also be interesting to carry out the resazurin assay for longer time (28 days for example) to further understand the cytotoxicity of the materials, as well as used human cells not only osteoblasts but also fibroblast to see if they performed a similar way. Then, after having a well-structured *in vitro* study, *in vivo* studies should be carried out to further progress the path of medical device certification, always based in the international ISO standards.

References

Agha, N. A., Feyerabend, F., Mihailova, B., Heidrich, S., Bismayer, U., & Willumeit-Romer, R. (2016). Magnesium degradation influenced by buffering salts in concentrations typical of in vitro and in vivo models. *Mater Sci Eng C Mater Biol Appl, 58*, 817-825. Retrieved from https://www.ncbi.nlm.nih.gov/pubmed/26478376. doi:10.1016/j.msec.2015.09.067

Akram, M. W., Fakhar, E. A. M., Atif, M., Butt, A. R., Asghar, A., Jamil, Y., . . . Wang, Z. M. (2018). In vitro evaluation of the toxic effects of MgO nanostructure in Hela cell line. *Sci Rep, 8*(1), 4576. Retrieved from https://www.ncbi.nlm.nih.gov/pubmed/29545644. doi:10.1038/s41598-018-23105-y

Al-Hazmi, F., Alnowaiser, F., Al-Ghamdi, A. A., Al-Ghamdi, A. A., Aly, M. M., Al-Tuwirqi, R. M., & El-Tantawy, F. (2012). A new large - Scale synthesis of magnesium oxide nanowires: Structural and antibacterial properties. *Superlattices Microstruct, 52*(2), 200-209. Retrieved from https://www.ncbi.nlm.nih.gov/pubmed/24748719. doi:10.1016/j.spmi.2012.04.013

An, Y. H., & Friedman, R. J. (1998). Concise review of mechanisms of bacterial adhesion to biomaterial surfaces. *J Biomed Mater Res, 43*(3), 338-348.

Antimicrobial Resistance: Tackling a crisis for the health and wealth of nations. (2014). Retrieved from Review on Antimicrobial Resistance: https://amrreview.org/

Aruoja, V., Pokhrel, S., Sihtmäe, M., Mortimer, M., Mädler, L., & Kahru, A. (2015). Toxicity of 12 metal-based nanoparticles to algae, bacteria and protozoa. *Environmental Science: Nano, 2*(6), 630-644. doi:10.1039/c5en00057b

Azam, A., Ahmed, A. S., Oves, M., Khan, M. S., Habib, S. S., & Memic, A. (2012). Antimicrobial activity of metal oxide nanoparticles against Gram-positive and Gram-negative bacteria: a comparative study. *Int J Nanomedicine, 7*, 6003-6009. Retrieved from https://www.ncbi.nlm.nih.gov/pubmed/23233805. doi:10.2147/IJN.S35347

Balraj, B., Senthilkumar, N., Vetha Potheher, I., & Arulmozhi, M. (2018). Characterization, antibacterial, anti-arthritic and in-vitro cytotoxic potentials of biosynthesized Magnesium Oxide nanomaterial. *Materials Science and Engineering: B, 231*, 121-127. doi:10.1016/j.mseb.2018.10.011

Barbeck, M., Dard, M., Kokkinopoulou, M., Markl, J., Booms, P., Sader, R. A., . . . Ghanaati, S. (2015). Small-sized granules of biphasic bone substitutes support fast implant bed vascularization. *Biomatter, 5*, e1056943. Retrieved from https://www.ncbi.nlm.nih.gov/pubmed/26083163. doi:10.1080/21592535.2015.1056943

Berney, M., Hammes, F., Bosshard, F., Weilenmann, H.-U., & Egli, T. (2007). Assessment and Interpretation of Bacterial Viability by Using the LIVE/DEAD BacLight Kit in Combination with Flow Cytometry.

Applied and Environmental Microbiology, 73(10), 3283. Retrieved from http://aem.asm.org/content/73/10/3283.abstract. doi:10.1128/AEM.02750-06

Bernhardt, A., Dittrich, R., Lode, A., Despang, F., & Gelinsky, M. (2013). Nanocrystalline spherical hydroxyapatite granules for bone repair: in vitro evaluation with osteoblast-like cells and osteoclasts. *J Mater Sci Mater Med, 24*(7), 1755-1766. doi:10.1007/s10856-013-4933-2

Bindhu, M. R., Umadevi, M., Kavin Micheal, M., Arasu, M. V., & Abdullah Al-Dhabi, N. (2016). Structural, morphological and optical properties of MgO nanoparticles for antibacterial applications. *Materials Letters, 166*, 19-22. doi:10.1016/j.matlet.2015.12.020

Bonini, M. G., Rota, C., Tomasi, A., & Mason, R. P. (2006). The oxidation of 2',7'-dichlorofluorescin to reactive oxygen species: a self-fulfilling prophesy? *Free Radic Biol Med, 40*(6), 968-975. Retrieved from https://www.ncbi.nlm.nih.gov/pubmed/16540392. doi:10.1016/j.freeradbiomed.2005.10.042

Bose, S., & Tarafder, S. (2012). Calcium phosphate ceramic systems in growth factor and drug delivery for bone tissue engineering: a review. *Acta Biomater, 8*(4), 1401-1421. doi:10.1016/j.actbio.2011.11.017

Brydone, A. S., Meek, D., & Maclaine, S. (2010). Bone grafting, orthopaedic biomaterials, and the clinical need for bone engineering. *Proc Inst Mech Eng H, 224*(12), 1329-1343. doi:10.1243/09544119jeim770

Burg, K. J., Porter, S., & Kellam, J. F. (2000). Biomaterial developments for bone tissue engineering. *Biomaterials, 21*(23), 2347-2359.

Cacciotti, I. (2016). Cationic and Anionic Substitutions in Hydroxyapatite. In I. V. Antoniac (Ed.), *Handbook of Bioceramics and*

Biocomposites (pp. 145-211).

Campana, V., Milano, G., Pagano, E., Barba, M., Cicione, C., Salonna, G., . . . Logroscino, G. (2014). Bone substitutes in orthopaedic surgery: from basic science to clinical practice. *J Mater Sci Mater Med, 25*(10), 2445-2461. doi:10.1007/s10856-014-5240-2

Canillas, M., Pena, P., de Aza, A. H., & Rodríguez, M. A. (2017). Calcium phosphates for biomedical applications. *Boletín de la Sociedad Española de Cerámica y Vidrio, 56*(3), 91-112. doi:10.1016/j.bsecv.2017.05.001

Cathcart, R., Schwiers, E., & Ames, B. N. (1983). Detection of picomole levels of hydroperoxides using a fluorescent dichlorofluorescein assay. *Anal Biochem, 134*(1), 111-116.

Chagnot, C., Listrat, A., Astruc, T., & Desvaux, M. (2012). Bacterial adhesion to animal tissues: protein determinants for recognition of extracellular matrix components. *Cell Microbiol, 14*(11), 1687-1696. Retrieved from https://www.ncbi.nlm.nih.gov/pubmed/22882798. doi:10.1111/cmi.12002

Champion, E. (2013). Sintering of calcium phosphate bioceramics. *Acta Biomater, 9*(4), 5855-5875. Retrieved from https://www.ncbi.nlm.nih.gov/pubmed/23212081. doi:10.1016/j.actbio.2012.11.029

Chen, X., Zhong, Z., Xu, Z., Chen, L., & Wang, Y. (2010). 2',7'-Dichlorodihydrofluorescein as a fluorescent probe for reactive oxygen species measurement: Forty years of application and controversy. *Free Radic Res, 44*(6), 587-604. Retrieved from https://www.ncbi.nlm.nih.gov/pubmed/20370560. doi:10.3109/10715761003709802

Choi, O., & Hu, Z. (2008). Size Dependent and Reactive Oxygen Species Related Nanosilver Toxicity to Nitrifying Bacteria. *Environmental Science & Technology, 42*(12), 4583-4588. Retrieved from https://doi.org/10.1021/es703238h. doi:10.1021/es703238h

Coathup, M. J., Cai, Q., Campion, C., Buckland, T., & Blunn, G. W. (2013). The effect of particle size on the osteointegration of injectable silicate-substituted calcium phosphate bone substitute materials. *J Biomed Mater Res B Appl Biomater, 101*(6), 902-910. Retrieved from https://www.ncbi.nlm.nih.gov/pubmed/23362131. doi:10.1002/jbm.b.32895

Coelho, C. C., Araujo, R., Quadros, P. A., Sousa, S. R., & Monteiro, F. J. (2019). Antibacterial bone substitute of hydroxyapatite and magnesium oxide to prevent dental and orthopaedic infections. *Mater Sci Eng C Mater Biol Appl, 97*, 529-538. Retrieved from https://www.ncbi.nlm.nih.gov/pubmed/30678939. doi:10.1016/j.msec.2018.12.059

Combs, K., & Cox, K. (2018). Clinical outcomes involving patients that develop septic arthritis with methicillin sensitive staphylococcus aureus versus methicillin resistant staphylococcus aureus. *J Orthop, 15*(1), 9-12. Retrieved from https://www.ncbi.nlm.nih.gov/pubmed/29167605. doi:10.1016/j.jor.2017.11.007

Das, B., Moumita, S., Ghosh, S., Khan, M. I., Indira, D., Jayabalan, R., . . . Balasubramanian, P. (2018). Biosynthesis of magnesium oxide (MgO) nanoflakes by using leaf extract of Bauhinia purpurea and evaluation of its antibacterial property against Staphylococcus aureus. *Mater Sci Eng C Mater Biol Appl, 91*, 436-444. Retrieved from https://www.ncbi.nlm.nih.gov/pubmed/30033274. doi:10.1016/j.msec.2018.05.059

Davis, C. (2014). Enumeration of probiotic strains: Review of culture-dependent and alternative techniques to quantify viable bacteria. *J Microbiol Methods, 103*, 9-17. Retrieved from https://www.ncbi.nlm.nih.gov/pubmed/24814752. doi:10.1016/j.mimet.2014.04.012

De Santis, R., Guarino, V., & Ambrosio, L. (2019). Composite biomaterials for bone repair. In *Bone Repair Biomaterials* (pp. 273-299).

Denry, I., & Kuhn, L. T. (2016). Design and characterization of calcium phosphate ceramic scaffolds for bone tissue engineering. *Dent Mater, 32*(1), 43-53. doi:10.1016/j.dental.2015.09.008

Dimitriou, R., Jones, E., McGonagle, D., & Giannoudis, P. V. (2011). Bone regeneration: current concepts and future directions. *BMC medicine, 9*, 66-66. Retrieved from https://www.ncbi.nlm.nih.gov/pubmed/21627784. doi:10.1186/1741-7015-9-66

Dorozhkin, S. V. (2013). Calcium Orthophosphate-Based Bioceramics. *Materials (Basel), 6*(9), 3840-3942. Retrieved from https://www.ncbi.nlm.nih.gov/pubmed/28788309. doi:10.3390/ma6093840

Dorozhkin, S. V., & Epple, M. (2002). Biological and Medical Significance of Calcium Phosphates. *Angewandte Chemie International Edition, 41*(17), 3130-3146. Retrieved from https://doi.org/10.1002/1521-3773(20020902)41:17<3130::AID-ANIE3130>3.0.CO;2-1. doi:10.1002/1521-3773(20020902)41:17<3130::AID-ANIE3130>3.0.CO;2-1

Dumont, M., Kaysser-Pyzalla, A., Kostka, A., Sander, P., & Borbely, A. (2009). *Characterization of Sauropod bone structure*.

Ennis, W. J., Sui, A., & Bartholomew, A. (2013). Stem Cells and Healing: Impact on Inflammation. *Advances in wound care, 2*(7), 369-378. Retrieved from https://www.ncbi.nlm.nih.gov/pubmed/24587974. doi:10.1089/wound.2013.0449

Ercan, B., Kummer, K. M., Tarquinio, K. M., & Webster, T. J. (2011). Decreased Staphylococcus aureus biofilm growth on anodized nanotubular titanium and the effect of electrical stimulation. *Acta Biomaterialia, 7*(7), 3003-3012. Retrieved from

http://www.sciencedirect.com/science/article/pii/S1742706111001589. doi:https://doi.org/10.1016/j.actbio.2011.04.002

Eruslanov, E., & Kusmartsev, S. (2010). Identification of ROS using oxidized DCFDA and flow-cytometry. *Methods Mol Biol, 594*, 57-72. Retrieved from https://www.ncbi.nlm.nih.gov/pubmed/20072909. doi:10.1007/978-1-60761-411-1_4

Francolini, I., & Donelli, G. (2010). Prevention and control of biofilm-based medical-device-related infections. *FEMS Immunol Med Microbiol, 59*(3), 227-238. Retrieved from https://www.ncbi.nlm.nih.gov/pubmed/20412300. doi:10.1111/j.1574-695X.2010.00665.x

Fuchs, R. K., Thompson, W. R., & Warden, S. J. (2019). Bone biology. In *Bone Repair Biomaterials* (pp. 15-52).

Giannoudis, P. V., Dinopoulos, H., & Tsiridis, E. (2005). Bone substitutes: an update. *Injury, 36 Suppl 3*, S20-27. doi:10.1016/j.injury.2005.07.029

Gold, K., Slay, B., Knackstedt, M., & Gaharwar, A. K. (2018). Antimicrobial Activity of Metal and Metal-Oxide Based Nanoparticles. *Advanced Therapeutics, 1*(3). doi:10.1002/adtp.201700033

Gong, T., Xie, J., Liao, J., Zhang, T., Lin, S., & Lin, Y. (2015). Nanomaterials and bone regeneration. *Bone Res, 3*, 15029. doi:10.1038/boneres.2015.29

Gonzalez, J., Hou, R. Q., Nidadavolu, E. P. S., Willumeit-Romer, R., & Feyerabend, F. (2018). Magnesium degradation under physiological conditions - Best practice. *Bioact Mater, 3*(2), 174-185. Retrieved from https://www.ncbi.nlm.nih.gov/pubmed/29744455. doi:10.1016/j.bioactmat.2018.01.003

Gosheger, G., Hardes, J., Ahrens, H., Streitburger, A., Buerger, H., Erren, M., . . . Von Eiff, C. (2004). Silver-coated megaendoprostheses in a rabbit model--an analysis of the infection rate and toxicological side effects. *Biomaterials, 25*(24), 5547-5556. doi:10.1016/j.biomaterials.2004.01.008

Gristina, A. G. (1987). *Biomaterial-Centered Infection: Microbial Adhesion Versus Tissue Integration* (Vol. 237).

Hadjidakis, D. J., & Androulakis, I. I. (2006). Bone Remodeling. *Annals of the New York Academy of Sciences, 1092*(1), 385-396. Retrieved from https://doi.org/10.1196/annals.1365.035. doi:10.1196/annals.1365.035

Hannink, G., & Arts, J. J. (2011). Bioresorbability, porosity and mechanical strength of bone substitutes: what is optimal for bone regeneration? *Injury, 42 Suppl 2*, S22-25. doi:10.1016/j.injury.2011.06.008

Hatzenbuehler, J., & Pulling, T. J. (2011). Diagnosis and management of osteomyelitis. *Am Fam Physician, 84*(9), 1027-1033.

Hench, L. L., & Best, S. M. (2013). Ceramics, Glasses, and Glass-Ceramics. In *Biomaterials Science* (pp. 128-151).

Hetrick, E. M., & Schoenfisch, M. H. (2006). Reducing implant-related infections: active release strategies. *Chem Soc Rev, 35*(9), 780-789. doi:10.1039/b515219b

Huang, L., Li, D. Q., Lin, Y. J., Wei, M., Evans, D. G., & Duan, X. (2005). Controllable preparation of Nano-MgO and investigation of its bactericidal properties. *J Inorg Biochem, 99*(5), 986-993. Retrieved from https://www.ncbi.nlm.nih.gov/pubmed/15833320. doi:10.1016/j.jinorgbio.2004.12.022

Iqbal, H. M. N., & Keshavarz, T. (2017). 13 - The challenge of biocompatibility evaluation of biocomposites. In L. Ambrosio (Ed.), *Biomedical Composites (Second Edition)* (pp. 303-334): Woodhead Publishing.

Ishikawa, K., Hoshino, E., & Furukawa, K. (2017). Staphylococcus aureus Bacteremia due to Central Venous Catheter Infection: A Clinical Comparison of Infections Caused by Methicillin-Resistant and Methicillin-Susceptible Strains. *Open Forum Infectious Diseases, 4*(suppl_1), S563-S564. Retrieved from https://doi.org/10.1093/ofid/ofx163.1473. doi:10.1093/ofid/ofx163.1473

ISO 10993-14. (2001). In *Biological evaluation of medical devices - Part 14: Identification and quantification of degradation products from ceramics*.

Jayakumar, P., & Di Silvio, L. (2010). Osteoblasts in bone tissue engineering. *Proc Inst Mech Eng H, 224*(12), 1415-1440. doi:10.1243/09544119jeim821

Jin, T., & He, Y. (2011). Antibacterial activities of magnesium oxide (MgO) nanoparticles against foodborne pathogens. *Journal of Nanoparticle Research, 13*(12), 6877-6885. doi:10.1007/s11051-011-0595-5

Jones, J. R. (2006). Observing cell response to biomaterials. *Materials Today, 9*(12), 34-43. Retrieved from http://www.sciencedirect.com/science/article/pii/S1369702106717412. doi:https://doi.org/10.1016/S1369-7021(06)71741-2

Jones, N., Ray, B., Ranjit, K. T., & Manna, A. C. (2008). Antibacterial activity of ZnO nanoparticle suspensions on a broad spectrum of microorganisms. *FEMS Microbiol Lett, 279*(1), 71-76. Retrieved from https://www.ncbi.nlm.nih.gov/pubmed/18081843. doi:10.1111/j.1574-6968.2007.01012.x

Karavolos, M. H., Horsburgh, M. J., Ingham, E., & Foster, S. J. (2003). Role and regulation of the superoxide dismutases of Staphylococcus aureus. *Microbiology, 149*(Pt 10), 2749-2758. Retrieved from https://www.ncbi.nlm.nih.gov/pubmed/14523108. doi:10.1099/mic.0.26353-0

Katsikogianni, M., & Missirlis, Y. F. (2004). Concise review of mechanisms of bacterial adhesion to biomaterials and of techniques used in estimating bacteria-material interactions. *Eur Cell Mater, 8*, 37-57.

Keer, J. T., & Birch, L. (2003). Molecular methods for the assessment of bacterial viability. *Journal of Microbiological Methods, 53*(2), 175-183. doi:10.1016/s0167-7012(03)00025-3

Kokubo, T., & Takadama, H. (2006). How useful is SBF in predicting in vivo bone bioactivity? *Biomaterials, 27*(15), 2907-2915. Retrieved from https://www.ncbi.nlm.nih.gov/pubmed/16448693. doi:10.1016/j.biomaterials.2006.01.017

Krishnamoorthy, K., Manivannan, G., Kim, S. J., Jeyasubramanian, K., & Premanathan, M. (2012). Antibacterial activity of MgO nanoparticles based on lipid peroxidation by oxygen vacancy. *Journal of Nanoparticle Research, 14*(9). doi:10.1007/s11051-012-1063-6

Leung, Y. H., Ng, A. M., Xu, X., Shen, Z., Gethings, L. A., Wong, M. T., . . . Leung, F. C. (2014). Mechanisms of antibacterial activity of MgO: non-ROS mediated toxicity of MgO nanoparticles towards Escherichia coli. *Small, 10*(6), 1171-1183. Retrieved from https://www.ncbi.nlm.nih.gov/pubmed/24344000. doi:10.1002/smll.201302434

Liu, X., Yang, H., Xiong, P., Li, W., Huang, H.-H., & Zheng, Y. (2019). Comparative studies of Tris-HCl, HEPES and NaHCO3/CO2 buffer systems on the biodegradation behaviour of pure Zn in NaCl and SBF solutions. *Corrosion Science*. doi:10.1016/j.corsci.2019.05.018

Lobo, S. E., & Arinzeh, T. L. (2010). Biphasic Calcium Phosphate Ceramics for Bone Regeneration and Tissue Engineering Applications. *Materials, 3*(2), 815-826. Retrieved from https://www.ncbi.nlm.nih.gov/pmc/articles/PMC5513510/. doi:10.3390/ma3020815

Mackie, E. J. (2003). Osteoblasts: novel roles in orchestration of skeletal architecture. *Int J Biochem Cell Biol, 35*(9), 1301-1305.

Maiti, S., Jana, S., & Jana, S. (2017). Biocomposites in therapeutic application. In *Biopolymer-Based Composites* (pp. 1-29).

Makhluf, S., Dror, R., Nitzan, Y., Abramovich, Y., Jelinek, R., & Gedanken, A. (2005). Microwave-Assisted Synthesis of Nanocrystalline MgO and Its Use as a Bacteriocide. *Advanced Functional Materials, 15*(10), 1708-1715. doi:10.1002/adfm.200500029

Marsh, A. C., Chamorro, N. P., & Chatzistavrou, X. (2019). Long-term performance and failure of orthopedic devices. In *Bone Repair Biomaterials* (pp. 379-410).

Matassi, F., Nistri, L., Chicon Paez, D., & Innocenti, M. (2011). New biomaterials for bone regeneration. *Clinical cases in mineral and bone metabolism : the official journal of the Italian Society of Osteoporosis, Mineral Metabolism, and Skeletal Diseases, 8*(1), 21-24. Retrieved from https://www.ncbi.nlm.nih.gov/pubmed/22461799.

Mirhosseini, M., & Afzali, M. (2016). Investigation into the antibacterial behavior of suspensions of magnesium oxide nanoparticles in combination with nisin and heat against Escherichia coli and Staphylococcus aureus in milk. *Food Control, 68*, 208-215. doi:10.1016/j.foodcont.2016.03.048

Montanaro, L., Speziale, P., Campoccia, D., Ravaioli, S., Cangini, I., Pietrocola, G., . . . Arciola, C. R. (2011). Scenery of Staphylococcus implant infections in orthopedics. *Future Microbiol, 6*(11), 1329-1349. doi:10.2217/fmb.11.117

Moriarty, T. F., Schlegel, U., Perren, S., & Richards, R. G. (2010). Infection in fracture fixation: can we influence infection rates through implant design? *J Mater Sci Mater Med, 21*(3), 1031-1035. doi:10.1007/s10856-009-3907-x

Nguyen, N. T., Grelling, N., Wetteland, C. L., Rosario, R., & Liu, H. (2018). Antimicrobial Activities and Mechanisms of Magnesium Oxide Nanoparticles (nMgO) against Pathogenic Bacteria, Yeasts, and Biofilms. *Sci Rep, 8*(1), 16260. Retrieved from https://www.ncbi.nlm.nih.gov/pubmed/30389984. doi:10.1038/s41598-018-34567-5

Nothdurft, F. P., Fontana, D., Ruppenthal, S., May, A., Aktas, C., Mehraein, Y., . . . Kaestner, L. (2015). Differential Behavior of Fibroblasts and Epithelial Cells on Structured Implant Abutment Materials: A Comparison of Materials and Surface Topographies. *Clin Implant Dent Relat Res, 17*(6), 1237-1249. doi:10.1111/cid.12253

O'Brien, J., Wilson, I., Orton, T., & Pognan, F. (2000). Investigation of the Alamar Blue (resazurin) fluorescent dye for the assessment of mammalian cell cytotoxicity. *Eur J Biochem, 267*(17), 5421-5426.

Oh, S., Oh, N., Appleford, M., & Ong, J. L. (2006). Bioceramics for Tissue Engineering - A Review. *American Journal of Biochemistry and Biotechnology 2 (2)*, 49-56.

Ohira, T., & Yamamoto, O. (2012). Correlation between antibacterial activity and crystallite size on ceramics. *Chemical Engineering Science, 68*(1), 355-361. doi:10.1016/j.ces.2011.09.043

Perl, T. M., Cullen, J. J., Wenzel, R. P., Zimmerman, M. B., Pfaller, M. A., Sheppard, D., . . . Herwaldt, L. A. (2002). Intranasal Mupirocin to Prevent Postoperative Staphylococcus aureus Infections. *New*

England Journal of Medicine, 346(24), 1871-1877. Retrieved from https://doi.org/10.1056/NEJMoa003069. doi:10.1056/NEJMoa003069

Pietrzak, W. S. (2008). Musculoskeletal Tissue Regeneration: Biological Materials and Methods. In (pp. 161-162): Humana Press, New Jersey.

Porter, J. R., Ruckh, T. T., & Popat, K. C. (2009). Bone tissue engineering: A review in bone biomimetics and drug delivery strategies. *Biotechnology Progress, 25*(6), 1539-1560. Retrieved from https://doi.org/10.1002/btpr.246. doi:10.1002/btpr.246

Prasad, K., Bazaka, O., Chua, M., Rochford, M., Fedrick, L., Spoor, J., . . . Bazaka, K. (2017). Metallic Biomaterials: Current Challenges and Opportunities. *Materials (Basel), 10*(8). doi:10.3390/ma10080884

Raucci, M. G., Guarino, V., & Ambrosio, L. (2012). Biomimetic strategies for bone repair and regeneration. *Journal of functional biomaterials, 3*(3), 688-705. Retrieved from https://www.ncbi.nlm.nih.gov/pubmed/24955638. doi:10.3390/jfb3030688

Rho, J.-Y., Kuhn-Spearing, L., & Zioupos, P. (1998). Mechanical properties and the hierarchical structure of bone. *Medical Engineering & Physics, 20*(2), 92-102. Retrieved from http://www.sciencedirect.com/science/article/pii/S1350453398000071. doi:https://doi.org/10.1016/S1350-4533(98)00007-1

Ribeiro, M., Monteiro, F. J., & Ferraz, M. P. (2012). Infection of orthopedic implants with emphasis on bacterial adhesion process and techniques used in studying bacterial-material interactions. *Biomatter, 2*(4), 176-194. Retrieved from https://www.ncbi.nlm.nih.gov/pubmed/23507884. doi:10.4161/biom.22905

Riss, T. L., Moravec, R. A., Niles, A. L., Duellman, S., Benink, H. A., Worzella, T. J., & Minor, L. (2013 May 1 [Updated 2016 Jul 1]). Cell Viability assays. In C. N. Sittampalam GS, Brimacombe K, et al. (Ed.), *Assay Guidance Manual [Internet]* [Bethesda (MD): Eli Lilly & Company and the National Center for Advancing Translational Sciences; 2004-.]. Retrieved from https://www.ncbi.nlm.nih.gov/books/NBK144065/

Rochford, E. T., Richards, R. G., & Moriarty, T. F. (2012). Influence of material on the development of device-associated infections. *Clin Microbiol Infect, 18*(12), 1162-1167. doi:10.1111/j.1469-0691.2012.04002.x

Rudin, A., & Choi, P. (2013). Chapter 13 - Biopolymers. In A. Rudin & P. Choi (Eds.), *The Elements of Polymer Science & Engineering (Third Edition)* (pp. 521-535). Boston: Academic Press.

Sakai, S., Anada, T., Tsuchiya, K., Yamazaki, H., Margolis, H. C., & Suzuki, O. (2016). Comparative study on the resorbability and dissolution behavior of octacalcium phosphate, beta-tricalcium phosphate, and hydroxyapatite under physiological conditions. *Dent Mater J, 35*(2), 216-224. Retrieved from https://www.ncbi.nlm.nih.gov/pubmed/27041011. doi:10.4012/dmj.2015-255

Samavedi, S., Whittington, A. R., & Goldstein, A. S. (2013). Calcium phosphate ceramics in bone tissue engineering: a review of properties and their influence on cell behavior. *Acta Biomater, 9*(9), 8037-8045. doi:10.1016/j.actbio.2013.06.014

Sawai, J. (2003). Quantitative evaluation of antibacterial activities of metallic oxide powders (ZnO, MgO and CaO) by conductimetric assay. *Journal of Microbiological Methods, 54*(2), 177-182. doi:10.1016/s0167-7012(03)00037-x

Sawai, J., Igarashi, H., Hashimoto, A., Kokugan, T., & Shimizu, M. (1996). Effect of Particle Size and Heating Temperature of Ceramic Powders on Antibacterial Activity of Their Slurries. *JOURNAL OF CHEMICAL ENGINEERING OF JAPAN, 29*(2), 251-256. doi:10.1252/jcej.29.251

Sawai, J., Kojima, H., Igarashi, H., Hashimoto, A., Shoji, S., Sawaki, T., . . . Shimizu, M. (2000). *Antibacterial Characteristics of Magnesium Oxide Powder* (Vol. 16).

Schieker, M., Seitz, H., Drosse, I., Seitz, S., & Mutschler, W. (2006). *Biomaterials as Scaffold for Bone Tissue Engineering* (Vol. 32).

Setsukinai, K., Urano, Y., Kakinuma, K., Majima, H. J., & Nagano, T. (2003). Development of novel fluorescence probes that can reliably detect reactive oxygen species and distinguish specific species. *J Biol Chem, 278*(5), 3170-3175. Retrieved from https://www.ncbi.nlm.nih.gov/pubmed/12419811. doi:10.1074/jbc.M209264200

Stewart, P. S., & William Costerton, J. (2001). Antibiotic resistance of bacteria in biofilms. *The Lancet, 358*(9276), 135-138. doi:10.1016/s0140-6736(01)05321-1

Stoimenov, P. K., Klinger, R. L., Marchin, G. L., & Klabunde, K. J. (2002). Metal Oxide Nanoparticles as Bactericidal Agents. *Langmuir, 18*(17), 6679-6686. doi:10.1021/la0202374

Suresh, M. K., Biswas, R., & Biswas, L. (2019). An update on recent developments in the prevention and treatment of Staphylococcus aureus biofilms. *Int J Med Microbiol, 309*(1), 1-12. Retrieved from https://www.ncbi.nlm.nih.gov/pubmed/30503373. doi:10.1016/j.ijmm.2018.11.002

Tande, A. J., & Patel, R. (2014). Prosthetic joint infection. *Clin Microbiol Rev, 27*(2), 302-345. Retrieved from https://www.ncbi.nlm.nih.gov/pubmed/24696437. doi:10.1128/CMR.00111-13

Tong, S. Y., Davis, J. S., Eichenberger, E., Holland, T. L., & Fowler, V. G., Jr. (2015). Staphylococcus aureus infections: epidemiology, pathophysiology, clinical manifestations, and management. *Clin Microbiol Rev, 28*(3), 603-661. Retrieved from https://www.ncbi.nlm.nih.gov/pubmed/26016486. doi:10.1128/CMR.00134-14

Trampuz, A., & Widmer, A. F. (2006). Infections associated with orthopedic implants. *Curr Opin Infect Dis, 19*(4), 349-356. doi:10.1097/01.qco.0000235161.85925.e8

Valletregi, M. (2004). Calcium phosphates as substitution of bone tissues. *Progress in Solid State Chemistry, 32*(1-2), 1-31. doi:10.1016/j.progsolidstchem.2004.07.001

Vidic, J., Stankic, S., Haque, F., Ciric, D., Le Goffic, R., Vidy, A., . . . Delmas, B. (2013). Selective antibacterial effects of mixed ZnMgO nanoparticles. *J Nanopart Res, 15*(5), 1595. Retrieved from https://www.ncbi.nlm.nih.gov/pubmed/23710129. doi:10.1007/s11051-013-1595-4

von Eiff, C., Jansen, B., Kohnen, W., & Becker, K. (2005). Infections associated with medical devices: pathogenesis, management and prophylaxis. *Drugs, 65*(2), 179-214. doi:10.2165/00003495-200565020-00003

Wang, H.-S. (2016). Development of fluorescent and luminescent probes for reactive oxygen species. *TrAC Trends in Analytical Chemistry, 85*, 181-202. doi:10.1016/j.trac.2016.09.006

Wang, P., Zhao, L., Liu, J., Weir, M. D., Zhou, X., & Xu, H. H. (2014). Bone tissue engineering via nanostructured calcium phosphate biomaterials and stem cells. *Bone Res, 2*, 14017. doi:10.1038/boneres.2014.17

Wang, W., & Yeung, K. W. K. (2017). Bone grafts and biomaterials substitutes for bone defect repair: A review. *Bioact Mater, 2*(4), 224-247. doi:10.1016/j.bioactmat.2017.05.007

Wetteland, C. L., Nguyen, N. Y., & Liu, H. (2016). Concentration-dependent behaviors of bone marrow derived mesenchymal stem cells and infectious bacteria toward magnesium oxide nanoparticles. *Acta Biomater, 35*, 341-356. Retrieved from https://www.ncbi.nlm.nih.gov/pubmed/26923529. doi:10.1016/j.actbio.2016.02.032

Williams, D. F. (1987). *Definitions in biomaterials : proceedings of a consensus conference of the European Society for Biomaterials, Chester, England, March 3-5, 1986*, Amsterdam; New York.

Wright, J. A., & Nair, S. P. (2010). Interaction of staphylococci with bone. *Int J Med Microbiol, 300*(2-3), 193-204. Retrieved from https://www.ncbi.nlm.nih.gov/pubmed/19889575. doi:10.1016/j.ijmm.2009.10.003

Xia, T., Kovochich, M., Brant, J., Hotze, M., Sempf, J., Oberley, T., . . . Nel, A. E. (2006). Comparison of the abilities of ambient and manufactured nanoparticles to induce cellular toxicity according to an oxidative stress paradigm. *Nano Lett, 6*(8), 1794-1807. Retrieved from https://www.ncbi.nlm.nih.gov/pubmed/16895376. doi:10.1021/nl061025k

Yamamoto, O. (2001). Influence of particle size on the antibacterial activity of zinc oxide. *International Journal of Inorganic Materials, 3*(7), 643-646. Retrieved from http://www.sciencedirect.com/science/article/pii/S1466604901001970. doi:https://doi.org/10.1016/S1466-6049(01)00197-0

Yamamoto, O., Ohira, T., Alvarez, K., & Fukuda, M. (2010). Antibacterial characteristics of CaCO3–MgO composites. *Materials Science and Engineering: B, 173*(1-3), 208-212. doi:10.1016/j.mseb.2009.12.007

Yang, D., Wijenayaka, A. R., Solomon, L. B., Pederson, S. M., Findlay, D. M., Kidd, S. P., & Atkins, G. J. (2018). Novel Insights into Staphylococcus aureus Deep Bone Infections: the Involvement of Osteocytes. *MBio, 9*(2). Retrieved from https://www.ncbi.nlm.nih.gov/pubmed/29691335. doi:10.1128/mBio.00415-18

Yeong, K. C. B., Wang, J., & Ng, S. C. (2001). Mechanochemical synthesis of nanocrystalline hydroxyapatite from CaO and CaHPO4. *Biomaterials, 22*(20), 2705-2712. Retrieved from http://www.sciencedirect.com/science/article/pii/S014296120000257X. doi:https://doi.org/10.1016/S0142-9612(00)00257-X

Yunus Basha, R., Sampath Kumar, T. S., & Doble, M. (2015). Design of biocomposite materials for bone tissue regeneration. *Mater Sci Eng C Mater Biol Appl, 57*, 452-463. Retrieved from https://www.ncbi.nlm.nih.gov/pubmed/26354284. doi:10.1016/j.msec.2015.07.016

Zimmerli, W. (2014). Clinical presentation and treatment of orthopaedic implant-associated infection. *J Intern Med, 276*(2), 111-119. doi:10.1111/joim.12233

Annexes

Annex A: Magnesium calculations from the degradation tests

1. Calculation of the Mg concentration present in the SBF solution:

To prepare 1L of SBF it was used 0,311g of $MgCl_2 \cdot 6H_2O$ (M=203,303 g/mol), which is equivalent a $n = \frac{m}{M} = \frac{0{,}311g}{203{,}303\ g/mol} = 1{,}5297 \times 10^{-3}\ mol$. Knowing that the molar mass (M) of the magnesium is 24,305 g/mol it is possible to calculate its mass in the solution: $m = n \times M = 1{,}5297 \times 10^{-3}\ mol \times 24{,}305\ g/mol = 0{,}03718\ g$ of Mg.

In 3,5mL of SBF (volume added to each falcon in the experiment): $m = \frac{0{,}0035\ L \times 0{,}03718\ g}{1\ L} = 1{,}3013 \times 10^{-4} g = 0{,}13013\ mg$ of Mg.

Finally, the [Mg] in the SBF volume used $= \frac{0{,}13013\ mg}{0{,}0035\ L} = 37{,}18\ mg/L.$

Having the weight of magnesium present in the SBF solution, and assuming a total volume of 3,5 mL, it is possible to subtract this value from the total values obtained from the ICP analysis, in order to obtain the results for the magnesium content derived from the materials only.

2. Demonstration of the calculations of the percentage of magnesium oxide released from the 3 wt% materials in the degradation tests

Using the data from the three replicates of the 3 wt% MgO 900 °C samples from the study performed according to the ISO standard (Tris-HCl solution) as an example, the steps and results obtained are presented in the next tables. First, it was calculated the 3 wt% of MgO from the material weighted at the beginning of the experiment.

Initial mass of the material (mg)	m_{MgO} in the material (mg) (3%)
171,3	5,139
171,5	5,145
171,4	5,142

Then, starting from the magnesium concentrations provided by the ICP analysis the following steps were performed:

$$[Mg](mg/L) \rightarrow m_{Mg}(mg) \rightarrow n_{Mg}(mol) \rightarrow m_{MgO}(mg) \rightarrow\rightarrow \%\ of\ MgO\ released$$

[Mg] (mg/L)	m_{Mg} (mg)	n_{Mg} (mol)	m_{MgO} in the solution (mg)	% mass of released MgO	Mean ± SD
145,7	0,5099	2,10E-05	0,8456	16,45	17,19% ± 0,64
155,1	0,5427	2,23E-05	0,9000	17,49	
156,1	0,5463	2,25E-05	0,9059	17,62	

M(MgO) = 40,304 g/mol

Using the first replica to demonstrate the calculations:

$$m_{Mg} = 145{,}7 mg/L \times 0{,}0035\ L = 0{,}5099\ mg \rightarrow n_{Mg} = \frac{0{,}5099\ \times 10^{-3} g}{24{,}305\ g/mol} = 2{,}098 \times 10^{-5} mol$$

$$m_{MgO\ in\ the\ solution} = 2{,}098 \times 10^{-5}\ mol \times 40{,}304\ g/mol = 8{,}456\ \times 10^{-4}\ g = 0{,}8456\ mg$$

$$\%\ mass\ of\ released\ MgO = \frac{m_{MgO\ in\ the\ solution}}{m_{MgO\ in\ the\ material}} \times 100 = \frac{0{,}8456\ mg}{5{,}139\ mg} \times 100 = 16{,}45\%$$

Table 6 – Weight percentage equivalent to the magnesium oxide content released from the 3 wt% MgO granules during the degradation tests in both solutions. The values are expressed as the mean percentage ± SD.

		Material		
Time-point	Solution	3 wt% MgO 900 °C	3 wt% MgO 1100 °C	3 wt% MgO 1300 °C
Day 1	Tris-HCl	17.2% ± 0.6	16.9% ± 1.4	7.6% ± 2.0
	SBF	15.4% ± 0.5	5.7% ± 0.3	0.5% ± 0.9
Day 3	Tris-HCl	41.6% ± 0.5	37.4% ± 8.1	32.2% ± 11.3
	SBF	31.3% ± 0.7	21.3% ± 0.9	6.0% ± 0.3
Day 7	Tris-HCl	63.9% ± 2.8	62.4% ± 4.1	47.5% ± 6.3
	SBF	42.9% ± 0.5	30.5% ± 1.3	5.4% ± 0.0
Day 14	Tris-HCl	71.6% ± 8.3	63.4% ± 4.1	58.1% ± 3.0
	SBF	48.3% ± 1.3	36.5% ± 0.8	4.9% ± 0.5
Day 21	Tris-HCl	74.9% ± 4.1	68.2% ± 4.1	60.1% ± 4.5
	SBF	53.1% ± 1.1	36.9% ± 1.7	5.1% ± 0.8
Day 28	Tris-HCl	71.1% ± 1.0	64.7% ± 2.1	55.8% ± 4.0
	SBF	52.9% ± 2.1	39.9% ± 2.4	5.3% ± 0.4